BUREAU OF — RECLAMATION

Final Report No. ST-2020-1754
Technical Report No. ENV-2020-83

Modeling of Cherry Creek Reservoir Pressure Flush

Science and Technology Program
Research and Development Office

U.S. Department of the Interior   **October 2020**

Mission Statements

The Department of the Interior (DOI) conserves and manages the Nation's natural resources and cultural heritage for the benefit and enjoyment of the American people, provides scientific and other information about natural resources and natural hazards to address societal challenges and create opportunities for the American people, and honors the Nation's trust responsibilities or special commitments to American Indians, Alaska Natives, and affiliated island communities to help them prosper.

The mission of the Bureau of Reclamation is to manage, develop, and protect water and related resources in an environmentally and economically sound manner in the interest of the American public.

Cover Photo: Cherry Creek Dam Intake (Reclamation)

REPORT DOCUMENTATION PAGE		*Form Approved* *OMB No. 0704-0188*
T1. REPORT DATE 10/2020	**T2. REPORT TYPE** Research	**T3. DATES COVERED 10/1/2019 – 9/30/2020**
T4. TITLE AND SUBTITLE **Modeling of Cherry Creek Reservoir Pressure Flush** **Final Report No. ST-2020-1754** **Technical Report No. ENV-2020-83**		**5a. CONTRACT NUMBER** FA880 (XXXR4524KS-RR4888FARD1803701)
		5b. GRANT NUMBER
		5c. PROGRAM ELEMENT NUMBER
6. AUTHOR(S) Yong G. Lai and Blair P. Greimann		**5d. PROJECT NUMBER:** 1754
		5e. TASK NUMBER
		5f. WORK UNIT NUMBER 86-68240
7. PERFORMING ORGANIZATION NAME(S) AND ADDRESS(ES) Sedimentation and River Hydraulics Group Technical Service Center, Bureau of Reclamation, Denver, CO 80225		**8. PERFORMING ORGANIZATION REPORT NUMBER**
9. SPONSORING / MONITORING AGENCY NAME(S) AND ADDRESS(ES) Research and Development Office U.S. Department of the Interior, Bureau of Reclamation, PO Box 25007, Denver CO 80225-0007		10. SPONSOR/MONITOR'S ACRONYM(S) R&D: Research and Development Office BOR/USBR: Bureau of Reclamation DOI: Department of the Interior
		11. SPONSOR/MONITOR'S REPORT NUMBER(S)
12. DISTRIBUTION / AVAILABILITY STATEMENT Final report can be downloaded from Reclamation's website: https://www.usbr.gov/research		
13. SUPPLEMENTARY NOTES		
14. ABSTRACT *(Maximum 200 words)* A numerical and empirical modeling study of pressure flushing through outlet works is reported at the Cherry Creek Dam and Reservoir, Denver, Colorado. Specifically, a 3D numerical model and empirical equations from laboratory experiments are developed and applied. The project is a joint collaborative effort among the Bureau of Reclamation, U.S. Army Corps of Engineers, and U.S. Geological Survey on the study of reservoir outlet maintenance activities. The 3D model is based on the solution of the Navier-Stokes equations along with sediment transport and mobile-bed modules. The numerical model results are compared with the field measurement results. Repeat land and bathymetric surveys, sediment sampling, and suspended sediment concentration measurement were made at the study site. The comparison allows us to evaluate the suitability of the numerical models for pressure flushing modeling. Model results may be used to evaluate whether improvements to gate operations may be made to increase the efficiency of sediment removal from the reservoir.		
15. SUBJECT TERMS Sediment Transport Modeling, Reservoir Sedimentation		
16. SECURITY CLASSIFICATION OF: U	**17. LIMITATION OF ABSTRACT** U	**18. NUMBER OF PAGES** 66	**19a. NAME OF RESPONSIBLE PERSON** Yong G. Lai
a. REPORT U **b. ABSTRACT** U **c. THIS PAGE** U			**19b. TELEPHONE NUMBER** 303-445-2560

S Standard Form 298 (Rev. 8/98)
P Prescribed by ANSI Std. 239-18

Mission Statements

The Department of the Interior (DOI) conserves and manages the Nation's natural resources and cultural heritage for the benefit and enjoyment of the American people, provides scientific and other information about natural resources and natural hazards to address societal challenges and create opportunities for the American people, and honors the Nation's trust responsibilities or special commitments to American Indians, Alaska Natives, and affiliated island communities to help them prosper.

The mission of the Bureau of Reclamation is to manage, develop, and protect water and related resources in an environmentally and economically sound manner in the interest of the American public.

Disclaimer

Information in this report may not be used for advertising or promotional purposes. The data and findings should not be construed as an endorsement of any product or firm by the Bureau of Reclamation, Department of Interior, or Federal Government. The products evaluated in the report were evaluated for purposes specific to the Bureau of Reclamation mission. Reclamation gives no warranties or guarantees, expressed or implied, for the products evaluated in this report, including merchantability or fitness for a particular purpose.

Acknowledgements

Modeling of Cherry Creek Reservoir Pressure Flush

Science and Technology Program
Research and Development Office
Final Report No. ST-2020-1754
Technical Report No. ENV-2020-83

prepared by

Technical Service Center

Yong Lai, Ph. D. Hydraulic Engineer, Sedimentation and River Hydraulics Group

Blair Greimann, Ph. D., Hydraulic Engineer, Sedimentation and River Hydraulics Group

Peer Review

Bureau of Reclamation

Research and Development Office

Science and Technology Program

Final Report No. ST-2020-1754

Technical Report No. ENV-2020-83

Modeling of Cherry Creek Reservoir Pressure Flush

_____

Prepared by: Yong Lai, Ph.D., Hydraulic Engineer, Sedimentation and River Hydraulics Group, Technical Service Center, Bureau of Reclamation, Denver, Colorado

_____

Prepared by: Blair Greimann, Ph.D., Hydraulic Engineer, Sedimentation and River Hydraulics Group, Technical Service Center, Bureau of Reclamation, Denver, Colorado

_____

Peer Review by: Jainchung Huang, Ph.D., Hydraulic Engineer, Sedimentation and River Hydraulics Group, Technical Service Center, Bureau of Reclamation, Denver, Colorado

Acronyms and Abbreviations

1D	one-dimensional
2D	two-dimensional
3D	three-dimensional
cfs	cubic feet per second
ft/hr-psf	Feet per hour per pounds per square foot
GIS	Geographic Information System
kg/m^3	kilograms per cubic meters
lb/ft^3	pounds per cubic foot
m^2/s	cubic meters per second
mg/L	milligrams per liter
mm	millimeters
Pa	Pascals
psf	pounds per square foot
Reclamation	Bureau of Reclamation
SMS	Aquaveo's Surface Water Modeling System
SRH-1D	Sedimentation River Hydraulics-One Dimension
SRH-2D	Sedimentation River Hydraulics-Two Dimensions
TSC	Technical Service Center
U^2RANS	Unstructured Unsteady Reynold's Averaged Navier Stokes
UPC	unstructured physical coordinate
VOF	volume of fluid
WSE	water surface elevation

Contents

Figures

Tables

Executive Summary

Cherry Creek Reservoir, a body of water located within Cherry Creek State Park, Colorado, serves as a flood mitigation measure and recreation area to its surroundings. The Bureau of Reclamation (Reclamation) is tasked with assessing the scour and its impact near the intakes during flushing. In this report, a numerical modeling study of pressure flushing through outlet works is reported at the Cherry Creek Dam and Reservoir, Denver, Colorado. Specifically, a three-dimensional (3D) numerical model is developed and applied. The project is a joint collaborative effort among the Reclamation, U.S. Army Corps of Engineers, and U.S. Geological Survey to study reservoir outlet maintenance activities. The 3D model is based on the solution of the Navier-Stokes equations along with sediment transport and mobile-bed modules. The numerical model results are compared with the field measurement results. Repeat land and bathymetric surveys, sediment sampling, and suspended sediment concentration measurement were made at the study site. The comparison allows us to evaluate the suitability of the numerical models for pressure flushing modeling. Model results may be used to evaluate whether improvements to gate operations may be made to increase the efficiency of sediment removal from the reservoir.

The numerical simulation of pressure flushing finds that the new 3D model based on the Navier-Stokes equations and the suspended cohesive sediment transport equation works well in simulating the pressure flushing process at the Cherry Creek Reservoir. The model predicted sediment release concentration is compared with the measured sediment concentration downstream in the river for both 2017 and 2018 releases. The agreement is reasonable and points to the potential of the 3D model for future pressure flushing applications. Further, the numerical model results suggest that the current 5-gate 2017 release schedule, with a maximum discharge of 250 cubic feet per second (cfs), is effective in removing the limited amount of sediments in front of the gates. If the maximum discharge would be 1,300 cfs like the 2018 release schedule, a 3-gate release— gates 3, 1 and 5, would be more efficient than the current 5-gate schedule. Other options to consider to maximize the efficiency of the flushing would be to flush every other year or to decrease the duration of the flushing. Most of the work performed by the flushing occurs immediately after the gates are opened.

An empirical analysis of the pressure flushing is also performed using equations developed from laboratory analyses. Empirical equations were shown to reasonably predict the area that is below or at the elevation of the sill of intake. However, the overall size of the scour cone and angle of the scour cone above the elevation of the sill of the intake was not predicted by the empirical analysis because the laboratory experiments could not predict the geotechnical processes that are important in defining the slope of the scour cone.

This study points also to future research and development direction and they are discussed in this report.

1. Background

Reservoir sedimentation and the operational problems of hydropower projects are becoming an increasingly prominent issue as new dam construction is becoming less viable. It was reported that, on average, 1% of the reservoir storage capacity was lost each year due to sedimentation (Morris and Fan, 1997; White, 2001; and Basson, 2007). Reservoir sedimentation is the key to attain the sustainable use of reservoirs. Proper sediment management is being sought to maintain the storage capacity of existing reservoirs and prolong the dam life.

At Reclamation, most dam facilities are approaching the age of 100 years. Reservoir sedimentation will become a major concern as Reclamation dams are aging, and it will limit Reclamation to meet the agency mission in the future. In fact, most Reclamation reservoirs will be affected by sedimentation. Often, the outlet was set at an estimated value after 100 years of sedimentation. This level is being exceeded at many reservoirs.

Some Reclamation reservoirs have already been impacted by the sedimentation and became a serious problem. For example, Paonia Reservoir, Colorado, has had difficulty in meeting project deliveries because of sediment and debris blockage at its intake. An appraisal level study is now underway to develop alternatives to sluice sediment through the reservoir in the hope of developing a sustainable alternative. Buffalo Bill Dam in Wyoming, a hydropower generation facility, is another example. They currently have two dam outlets (hydropower and river outlets) near each other and at the same elevation. They occasionally use the river outlet to flush sediment. The operation has been successful in creating enough of a cone of depression to maintain unobstructed hydropower intake. Reservoir drawdown is effective for sediment flushing but it is not feasible most of the times due to the need for power generation.

In other cases, reservoir sediment is beginning to approach to the intake elevation for either a penstock or water diversion. Facilities where reservoir sedimentation is starting to reduce project benefits include Black Canyon in Idaho, Elephant Butte in New Mexico, Summer in New Mexico, and Arrowrock in Idaho, among others. A gated intake at a lower elevation may be used to remove sediment in the vicinity of the gate and prevent sediment from entering the penstock or water diversion. Flushing through reservoir drawdown can be an efficient option to hydraulically remove the sediment downstream. Unfortunately, many reservoirs do not have the luxury to adopt the drawdown sluicing due to the large loss of water. For many large reservoirs, pressure flushing is the main viable option as it requires only a minimal amount of water.

Various sediment removal measures may be used; among them are the upstream watershed management, hydraulic flushing, sediment bypass tunnels, density current venting, and mechanical dredging (Shen, 1999). Hydraulic flushing is an economically attractive mean to manage sedimentation when low-level outlets exist for the reservoir. It is also one of the best methods through which the previously deposited sediment in the reservoir may be removed by opening the bottom outlets of the dam (Shen, 1990 and Madadi et al., 2017). Two types of hydraulic flushing may be used: the drawdown free-flow flushing and pressure flushing. The drawdown flushing is carried out by lowering the reservoir pool elevation to near the outlet level; it is a very effective technique for sediment removal. Drawdown flushing, however, is not always viable for large reservoirs as the stored water is needed for delivery commitment and/or power generation. For such reservoirs, pressure flushing is the main alternative. Pressure flushing in this report refers to the process where flushing is carried out when the reservoir water is maintained at a constant level well above the outlet. The effectiveness of pressure flushing, however, has long been viewed as low; only sediment in the vicinity of the outlet is removed during a pressure flushing (Fan and Morris, 1992 and Kantoush, 2008). Jansson and Erlingsson (2000), e.g., found that the scouring cone was limited in an area in the vicinity of the bottom outlet. Further, the pressure flushing schedule adopted—the timing, duration and release discharge—may impact the flushing efficiency in a significant way. Our understanding of pressure flushing is limited at present and often the design of an efficient flushing schedule is not science-based. The present study focuses primarily on pressure flushing and seek whether a science-based approach may be developed.

There are limited studies of pressure flushing. Most were replied on the experimental approach, using the physical model studies, to optimize the layout and design of the hydraulic structures of a project (Isaac et al. 2014). Some of the experimental studies are discussed below, among others.

Talebbeydokhti and Naghshineh (2004) conducted an experimental work using the physical model. They found that the amount of sediment flushed was a function of the release discharge, the water level and the flushing channel width. Emamgholizadeh et al. (2006) investigated the scour cone development with varying release flow and water depth above the outlet. It was observed that the scour cone volume and size increased with the release discharge and decreased with the water depth. Meshkati et al. (2009 and 2012) studied the time dependent process of the scour cone in a water storage reservoir and developed a set of non-dimensional relationships for the temporal variations of the scour cone dimensions. The effect of the outlet cross-section size was also investigated on the cone development. It was found that the cone size was a strong function of the outlet diameter. Powell and Khan (2012 and 2015) reported laboratory studies using circular outlets. They investigated the flow characteristics and the sediment transport, primarily the formation of vortices near the outlet. Ahadpour Dodaran et al. (2012)

conducted an experimental study to understand the effect of the frequency and location of a vibrating plate on the scour cone sized. They concluded that the vibrating plate had a positive effect on the scour cone size. Most experiments were carried out using the non-cohesive sediments. An exception was the work of Emamgholizadeh and Fathi-Moghadam (2014) who studied the cohesive sediment cone development. They reported that the scour cone volume and size decreased with an increase in the sediment bulk density. The bulk density reflects the compaction of the cohesive materials and produces different erodibility. It was found to be the most important parameter in comparison with discharge and water depth.

In recent studies, Kemble et al. (2017) reported hydraulic modeling to understand the scour cone development during pressure flushing for a run-of-the-river hydro-electric project. The experiment was done in a flume fitted with a single spillway bay; flushing discharge and water depth were varied. Using the dimensional analysis and measured data, special relations were developed for computing the dimensionless parameters of flushing cone geometry (depth and length) in the vicinity of outlet. These relations may be useful for project design purpose. In another study, Madadi et al. (2017) used the laboratory experiment to investigate whether a new outlet configuration might increase the pressure flushing efficiency. A projecting semicircular structure was connected to the upstream edge of the bottom outlet. It demonstrated that the proposed new outlet increased the sediment removal efficiency significantly in comparison with the traditional flushing without the projecting structure.

Hajikandi et al. (2018) compared difference equilibrium scour conditions between square and circular orifices. They found very similar non-dimensional scour shapes as Powell and Khan (2012), but that the scour length was 10 to 15 percent longer for a square orifice of the small cross-sectional area as a circular orifice. Similar to Powell and Khan (2012), the length and the width of the scour hole showed weak dependency on particle size. These results also extend the results of Powell and Khan (2012) to higher values of water depth to orifice diameters.

We believe that a cost-effective way for a science-based approach for pressure flushing is to resort to advanced numerical models. This leads to the present study question: *can we develop new capabilities and construct numerical models to assist in the design and operation of the low-level outlets for pressure sluicing?*

In the numerical modeling area, few studies were found with regard to pressure flushing, although free-flow drawdown flush has been simulated and reported by a number of researchers (e.g., one-dimensional [1D] modeling by Chang et al., 1996, Liu et al., 2004, and Huang et al., 2019; two-dimensional [2D] modeling by Lai and Greimann, 2012; and 3D modeling by Fang and Rodi, 2003 and Haun and Olsen, 2012). We decided to develop a new 3D modeling capability at Reclamation.

In the past, Reclamation's Technical Service Center (TSC), Sedimentation and River Hydraulics Group has developed several sediment transport models that have been used for many Reclamation projects. Sedimentation River Hydraulics-One Dimension (SRH-1D) (Huang and Greimann, 2012) is a one-dimensional hydraulic and sediment transport numerical model that simulates the cross-sectionally averaged sediment transport, erosion, and deposition. It is useful for large scale river studies and for reservoirs where drawdown sediment sluicing is the primary mechanism for sediment erosion. It has been applied to the Paonia Reservoir studies where drawdown sediment sluicing is currently being used to simulate a sustainable reservoir sediment management strategy. It has also been applied to dam removal studies where the dam is permanent removed.

Sedimentation River Hydraulics-Two Dimensions (SRH-2D) (Lai, 2008 and 2010 and Lai and Greimann, 2010) is a two-dimensional (2D) depth-averaged hydraulic and sediment transport model that simulates the depth-averaged sediment transport, erosion and deposition with a horizontal 2D mesh. SRH-2D has been widely used for numerous projects at Reclamation and also nationally and internationally. In general, 2D models are suitable for smaller-scale sediment transport problems such as around diversion structures or at specific river restoration projects. SRH-2D model has been applied to drawdown sluicing at reservoirs such as on the Klamath River, Elwha River and Ventura River. A version of SRH-2D has also been developed to predict the pressure flushing of the turbidity current that can occur in large reservoirs with high sediment concentrations. Successful applications of the model to turbidity current venting has been demonstrated at the Shihmen Reservoir, Taiwan, where sediment bypasses around reservoirs are being designed.

Unfortunately, the 1D and 2D models are not applicable to the pressure flushing cases, as both SRH-1D and SRH-2D assumed that the velocity is uniform throughout the depth. This is acceptable for river applications or where reservoirs are drawn down. When pressurized sediment flushing is being performed, this assumption prevents these models from being useful. A three-dimensional (3D) model is necessary for pressure flushing modeling.

Above review shows the lack of appropriate numerical modeling tools in the ability to simulate pressure flushing; few 3D modeling studies are known to us. Our current sediment models can only model flushing of sediment when the reservoir is drawdown completely and there is no appreciable reservoir pool left. There are no current 3D flow and sediment transport models that would meet Reclamation needs. Some potential 3D models were investigated include Flow3D, SIIM, and Delft3D. Wei et al (2014) detailed the sediment modeling capabilities of Flow3D, but as stated in their documentation, currently the Flow-3D model does not have the capabilities to simulate silt and clay. SIIM, documented by Olsen (2014), is one of the few 3D numerical models that has been

successfully used to estimate flushing of reservoir sediment but it was limited to drawdown flushing. This model has proven that it can adequately simulate some cases of reservoir flushing, but it is considered a research level code and is only supported by a single professor at the Norwegian University of Science and Technology. It is likely that the university will not continue to support the model after he leaves. Dleft3D, described at http://oss.deltares.nl/web/delft3d/research, has an open source version and has been widely used with some applications of reservoir sluicing. However, it has not been applied by Reclamation for sediment sluicing and its success is uncertain. Further, the model made the static pressure assumption and may not be accurate in pressure flushing modeling.

The objective of this research is to extend an existing 3D model to simulate the pressure flushing of sediment at reservoirs. The model is named U^2RANS which was originally developed at the University of Iowa (Lai et al., 2003). The model has undergone further development at Reclamation through funding provided by Taiwan Water Resources Agency. The new developments focused primarily on adapting U^2RANS for river and reservoir modeling. In this project, new efforts include the development of a suspended sediment transport module suitable for the pressure flushing modeling; the module is then coupled to the flow solver. The new extended model will be suitable for cases where the reservoir is near full but a low-level gate is opened to use pressure flushing to remove sediment in front of the gate. The model is modified to simulate the pressure flushing at the Cherry Creek Reservoir.

An empirical analysis of the pressure flushing is also performed using equations developed from previous studies to determine the usefulness of empirical analyses. The empirical equations are evaluated as to how to apply them to field situations similar to Cherry Creek.

In the following the model development and application to the Cherry Creek Reservoir are reported.

2. Numerical Model

2.1. Flow Equations

The 3D flow model U^{2}RANS has been developed and documented before (Lai et al. 2003). A brief description is provided herein.

The 3D flow model solves the following unsteady Reynolds averaged Navier-Stokes (RANS) equations:

$$\frac{\partial \rho}{\partial t} + \frac{\partial \rho U_j}{\partial x_j} = 0$$

$$\frac{\partial \rho U_i}{\partial t} + \frac{\partial \rho U_i U_j}{\partial x_j} = \frac{\partial}{\partial x_j}\left(\mu \frac{\partial U_i}{\partial x_j} + \tau_{ij}\right) - \frac{\partial P}{\partial x_i} + \rho g_i$$

Where:

> t is time;
> x_j is the j-th Cartesian coordinate;
> ρ is the water-sediment mixture density;
> U_j is the mean velocity components along the Cartesian coordinate x_j;
> $\tau_{ij} = -\rho\overline{u_i u_j}$ is the turbulence stress with u_j the j-th turbulent fluctuating velocity component;
> P is the mean pressure;
> μ is the mixture viscosity; and
> g_i is the i-th component of the acceleration due to gravity.

The above equation can also be cast in tensor form as:

$$\frac{\partial \rho}{\partial t} + \nabla \bullet \left(\rho \vec{V}\right) = 0$$

$$\frac{\partial \rho \vec{V}}{\partial t} + \nabla \bullet \left(\rho \vec{V}\vec{V}\right) = -\nabla P + \nabla \bullet \left(\mu \nabla \vec{V} - \vec{\vec{\tau}}\right) + \rho \vec{g}$$

A turbulence model is used to relate the Reynolds stress tensor τ_{ij} in the above equations to other variables. In this study, the standard two equation model, the k-ε model of Launder and Spalding (1974), is adopted. That is, the Reynolds stresses is related to the mean strain rate through a turbulent eddy viscosity as:

$$\tau_{ij} = \mu_t \left(\frac{\partial U_i}{\partial x_j} + \frac{\partial U_j}{\partial x_i} \right) - \frac{2}{3} \rho k \delta_{ij} \qquad \text{or}$$

$$\vec{\vec{\tau}} = \mu_t \left[\nabla \vec{V} + \left(\nabla \vec{V} \right)^T \right] - \frac{2}{3} \rho k \vec{\vec{I}}$$

Where:

δ_{ij} (or $\vec{\vec{I}}$) is the Kronecker delta (a unit tensor).

The eddy viscosity is obtained by:

$$\mu_t = C_\mu \rho \frac{k^2}{\varepsilon}$$

Where:
k is the turbulence kinetic energy and
ε is the turbulence dissipation rate.

The transport equations for k and ε for non-buoyant flows may be expressed as:

$$\frac{\partial \rho k}{\partial t} + \frac{\partial \rho U_j k}{\partial x_j} = \frac{\partial}{\partial x_j} \left((\mu + \frac{\mu_t}{\sigma_k}) \frac{\partial k}{\partial x_j} \right) + G - \rho \varepsilon$$

$$\frac{\partial \rho \varepsilon}{\partial t} + \frac{\partial \rho U_j \varepsilon}{\partial x_j} = \frac{\partial}{\partial x_j} \left((\mu + \frac{\mu_t}{\sigma_\varepsilon}) \frac{\partial \varepsilon}{\partial x_j} \right) + C_{\varepsilon 1} \frac{\varepsilon}{k} G - C_{\varepsilon 2} \rho \frac{\varepsilon^2}{k}$$

Where:

$G = \tau_{ij} \dfrac{\partial U_i}{\partial x_j}$ is the turbulence generation rate due to velocity strain rate.

The standard model constants take the following values:

$C_\mu = 0.09; \ C_{\varepsilon 1} = 1.44, \ C_{\varepsilon 2} = 1.92, \ \sigma_k = 1.0, \ \sigma_\varepsilon = 1.3$

Common boundary conditions encountered in hydraulic flow modeling include flow inlet, outlet, no-slip wall, symmetry, and free surface.

At a flow inlet, Cartesian velocity components or flow discharge are specified at mesh cell faces. Pressure is not an input and is determined by means of an extrapolation from the value at the mesh interior. These values of flow properties are used in solving the mass and momentum equations. The solution of the pressure correction equation requires no pressure boundary condition because mass fluxes on these boundaries are specified

8

and remain unchanged during the solution. Turbulence quantities, k and ε, are specified at an inlet as user inputs; they are less important in general as they primarily impact results near the inlet which is usually located far upstream from the interest area of the stream.

At a flow outlet, pressure is specified at the mesh cell faces while Cartesian velocity components and turbulence quantities are determined by means of an extrapolation from the values at the mesh interior. For the pressure-correction equation, the pressure increment is to zero at the outlet because pressure should not change during the solution.

At no-slip solid walls such as riverbeds, the standard wall-function approach is adopted based on the work of Launder and Spalding (1974). The wall function approach assumes that the nearest mesh cell center point is located within the inertial sublayer so that a theoretically derived log-law equation is valid. In the equation, the wall roughness may be taken into account. The log-law equation may be derived assuming the turbulence near a wall is in equilibrium. It is noted that the log-law is theoretically valid only if the first mesh point is located within the inertial sublayer. It is generally requited that the distance of the center of the first mesh cell near the wall (δ_1)satisfies $30 < \delta_1^+ = \dfrac{u_\tau \delta_1}{\nu} < 300$. As discussed by Liu (2014), $0.2k_s \leq \delta_1 \leq 0.1h$ is also required for rough beds of an open channel flows (h is water depth).

Stumpp (2001) has evaluated a number of roughness treatment methods for stream flow simulations using U^{2}RANS model. Results were compared to a large number of experimental data with varying surface roughness. Based on the findings of Stumpp (2001), the formulation of the log-law adopted is:

$$\frac{u}{u_\tau} = \frac{1}{\kappa} \ln(\frac{z^+}{z_0})$$

$$z^+ = \frac{zu_\tau}{\nu} \qquad u_\tau = \sqrt{\frac{\tau_w}{\rho}}$$

Where:

κ is the von Karman constant (0.41),
z is the distance from the wall,
τ_w is the shear stress at the wall, and
z_0 is the wall roughness parameter.

The roughness parameter z_0 is linked to the geometric variation of wall surface unresolved by the mesh. The Cebeci and Bradshaw (1977) formula is adopted in which the roughness parameter is computed by:

$$z_0 = \exp\{-\kappa(5.2 - \Delta)\}$$

$$\Delta = \begin{cases} 0, & k_s^+ < 2.25 \\ \left[\ln(k_s^+)/\kappa - 3.3\right]\sin\{0.4258[\ln(k_s^+) - 0.811]\}, & 2.25 \leq k_s^+ < 90 \\ \ln(k_s^+)/\kappa - 3.3, & k_s^+ \geq 90 \end{cases}$$

$$k_s^+ = \frac{u_\tau k_s}{\nu}$$

Where:

k_s is the effective roughness height.

The roughness height is zero for the smooth wall and a user input for rough walls. It is recommended that users take it as a calibration parameter when data are available. k_s may be calibrated to match the observed water surface elevation at the upstream end of the stream inlet.

The roughness height k_s represents the root-mean-square value of the sub-grid bottom elevation fluctuations and is a function of both grain and form drags similar to the Manning's roughness coefficient used by the depth-averaged models. It reflects the influence of sediment grains, bed waves, and other energy losses. A wide range of guidelines have been suggested in the past. Wu et al. (2000) suggested that the roughness height may be taken to be one to three times the medium diameter of bed sediments for stationary flat beds. Van Rijn (1984), however, recommended to use $3\,d_{90}$. For stream beds with bed forms, the wave height should be added to the estimate of the roughness height which may led to more than 10 times the sediment size; one such formula was discussed by van Rijn (1984). We found that specification of the roughness height is very arbitrary at present and there is no consensus of the best way for all scenarios. At present, we suggest using $k_s = 3d_{50}$ as the default for flat beds, but higher values may be needed for scour simulation or in the field applications. It should be calibrated to match the measured shear stress, water elevation or scour depth in streams. We have found cases where the k_s value is much larger than the grain size of the bed (more than ten times).

At a no-slip wall, k and ε values are computed through the equilibrium assumption as follows:

$$k_W = \frac{u_\tau^2}{\sqrt{C_\mu}} \qquad\qquad \varepsilon_W = \frac{u_\tau^3}{\kappa\delta_1} = \frac{C_\mu^{3/4} k_W^{3/2}}{\kappa\delta_1}$$

Free surface may be treated with one of two approaches: the solid-lid method and the decoupled method. The solid-lid method treats the free surface as a slip boundary. The free surface itself is represented by the 3D mesh and the elevation can be either a constant value (flat) or estimated from the computed pressure distribution on the free surface (Lai et al., 2003). The solid-lid method has been widely used in 3D modeling of open channel flows. It is adequate for open channel flows with low Froude number (<0.3) and relatively small spatial variation of free surface elevation (Lai et al., 2003).

The second decoupled method obtains the free surface elevation using a set of equations apart from U^{2}RANS. For example, SRH-2D may be used to obtain the free surface. The decoupled method is implemented as follows. The free surface elevation is first computed with SRH-2D. U^{2}RANS modeling is then carried out by using the computed free surface elevation. The decoupled method is adequate for most open channel flows and lake/reservoir modeling; but the modeling process is inconvenient as a two-step modeling has to be performed. More sophisticated free surface computation methods are needed in future developments such as the Volume of Fluid (VOF) method or the level set method.

The free surface boundary condition is the same as the symmetry for the mass and momentum equations. That is, the velocity component normal to the surface is set to be zero while the normal derivative of the tangential velocity is zero. At present, zero wind speed is assumed at a free surface.

Turbulence equations need different boundary conditions for symmetry or free surface boundaries. At a symmetry the derivatives of both k and ε are set to zero normal along the normal direction of the boundary. At a free surface, we use the Dirichlet boundary condition for k and ε. This approach simplifies the model implementation as turbulence generation terms are not needed for the first cells touching the free surface. At a free surface, the following Dirichlet conditions are applied:

$$k_S = \frac{u_{\tau S}^2}{\sqrt{C_\mu}} \qquad\qquad \varepsilon_S = \frac{u_{\tau S}^3}{\kappa \delta_S}$$

Where:

$u_{\tau S}$ is the free surface friction velocity due to wind forcing (it is zero at present) and

δ_S is the normal distance from the cell centroid near the free surface to the free surface face.

2.2. Sediment Transport Equations

Sediment transported in rivers and reservoirs may be divided into four categories: wash load, suspended load, mixed load, and bed load. Wash load is transported through the modeling domain without interaction with those on the bed and is normally ignored. The suspended load is transported through the system in "suspended" mode in water column, but it has a non-zero fall velocity and may exchange sediments with the bed leading to a net effect of bed erosion or deposition. The bed load refers to the sediment that saltates and/or rolls along the bed as opposed to the suspended load in water column. The mixed load is defined as the sediment sizes that are transported in between the suspended and bed load forms. In terms of modeling effort, the mixed load is most demanding, followed by suspended load, wash load, and bed load.

In this study, a special suspended load module is developed into U²RANS. Only suspended load transport is considered as sediment deposits near the dam face are usually very fine. In general, suspended sediment may be divided into a number of size classes although only a single fine size is tested and applied in the present study. In general, each size class is transported in the system separately and independent of each other. The 3D transport of a suspended sediment size class, say size k, is governed by the following advection-diffusion equation derived from mass conservation:

$$\frac{\partial C_k}{\partial t} + \frac{\partial U C_k}{\partial x} + \frac{\partial V C_k}{\partial y} + \frac{\partial (W - \omega_k) C_k}{\partial z} =$$

$$\frac{\partial}{\partial x}\left(D_k \frac{\partial C_k}{\partial x}\right) + \frac{\partial}{\partial y}\left(D_k \frac{\partial C_k}{\partial y}\right) + \frac{\partial}{\partial z}\left(D_k \frac{\partial C_k}{\partial z}\right)$$

Where:
C_k is the volume concentration for sediment size class k (defined as ρ_k / ρ_S with ρ_k the mass concentration of size k and ρ_S the specific sediment density);

ω_k is the fall velocity for size k; and

D_k is the diffusivity.

 The specific density is assumed to be the same for all size classes.

The diffusivity is computed by:

$$D_k = \frac{v_T}{\sigma_{Ck}}$$

Where:
σ_{Ck} is the Schmidt parameter. For fine sand and cohesive sediments ($\leq 150 \mu m$) σ_{Ck} is usually found to be 1.0.

The unhindered fall velocity for non-cohesive sediments may be computed by a number of ways. One method is based on van Rijn (1993) as:

$$\omega_k = \frac{(\gamma - 1)gd_k^2}{18\nu} \qquad\qquad 65\mu m < d_k \le 100\mu m$$

$$\omega_k = \frac{10\nu}{d_k}\left(\sqrt{1 + \frac{0.01(\lambda - 1)gd_k^3}{\nu^2}} - 1\right) \qquad\qquad 100\mu m < d_k \le 1000\mu m$$

$$\omega_k = 1.1\sqrt{(\gamma - 1)gd_k} \qquad\qquad 1000\mu m < d_k$$

Where:

γ is the specific gravity of sediment ($= \rho_s / \rho_w$)

ν is the kinematic water viscosity (cubic meters per second [m²/s])

The unhindered fall velocity for cohesive sediments can be either the same as the non-cohesive sediments or a user provided value.

Boundary conditions are needed to solve the above suspended sediment concentration equation. At free surfaces, the net sediment concentration flux is set to zero; i.e.,

$$\omega_k C_k + D_{Vk}\frac{\partial C_k}{\partial z} = 0$$

At the stream or reservoir bed, the net sediment flux reflects the net sediment exchange rate with the bed; it is non-zero unless the flow has reached equilibrium. The net sediment flux with the bed is computed by:

$$\omega_k C_k + D_{Vk}\frac{\partial C_k}{\partial z} = D_k - E_k$$

Where:
$D_k = \omega_k C_k$ is the deposition rate and
E_k is the sediment entrainment rate, respectively.

The entrainment rate for the non-cohesive size class may be computed by:

$$E_k = \begin{cases} \omega_k C_k^* & \text{loose bed with unlimted supply} \\ \min(\omega_k C_k^*, \omega_k C_k) & \text{fixed bed without supply} \end{cases}$$

In the above, the entrainment rate is proportional to the local equilibrium concentration (C_k^*) near the bed. The equilibrium concentration is determined by an empirical equation derived from experimental data. For a fixed bed without sediment supply, only deposition is allowed. The equilibrium concentration equation proposed by Zyserman and Fredsøe (1994) may be adopted. It computes the equilibrium concentration as follows:

$$C_{b*} = \frac{0.331(\theta - 0.045)^{1.75}}{1 + \dfrac{0.331}{0.46}(\theta - 0.045)^{1.75}}$$

$$\delta = 2d$$

$$\theta = \frac{u_\tau^2}{(\gamma - 1)gd} \qquad \text{(Shields parameter)}$$

Where:
d is the sediment diameter and
δ is the reference height, which is assumed to be twice the sediment diameter.

In the present study, the bed is primarily cohesive. For cohesive sediment, the sediment entrainment rate is computed as:

$$E_k = p_k \varepsilon (\tau_b - \tau_c)$$

Where:

p_k is the volume fraction of the cohesive size class on the bed,
ε is the erodibility,
τ_c is the critical shear stress of the cohesive bed,
and τ_b is the bed shear stress.

It is noted that the erodibility may not be a constant for cohesive sediment. For example, two erosion modes may exist, one is the surface erosion and the other is the mass erosion (Partheniades, 1965). Surface erosion has a smaller erodibility and occurs when bed shear stress is just above a relatively critical value. At higher bed shear stress levels, mass erosion may occur when a layer of bed material is lifted and eroded once bed shear stress exceeds the bulk shear strength of the bed material. The erodibility can be much higher than the surface erosion mode. Only a single erodibility is implemented in the present study.

Deposition of cohesive sediments depend on a number of processes and it occurs when bed shear stress is less than a critical value. According to the laboratory study of cohesive sediment depositional behaviors by Mehta and Partheniades (1973), deposition is controlled by shear stress on the bed, turbulence near the bed, settling velocity, sediment

type, flow depth, suspended concentration, and ionic constitution. Two deposition processes may be modeled: full and partial. The deposition rate is computed as follows:

$$
\begin{cases}
D_k = \omega_k \left(1 - \dfrac{\tau_b}{\tau_{ref}}\right) \; If \; \tau_b \le \tau_f \\
D_k = \omega_k \left(1 - \dfrac{\tau_b}{\tau_p}\right)\left(1 - \dfrac{C_{eq}}{C_k}\right) \; If \; \tau_f < \tau_b < \tau_p \; and \; C_k > C_{eq} \\
D_k = 0 \; If \; \tau_b \ge \tau_p \; or \; C_k \le C_{eq}
\end{cases}
$$

$$
\tau_{ref} = \frac{\tau_f \, \tau_p}{\chi \, \tau_f + (1-\chi)\tau_p} \qquad\qquad \chi = 1 - \frac{C_{eq}}{C_k}
$$

Where:
τ_f is the critical bed shear stress below which full deposition dominates,
τ_p is the critical stress above which no deposition happens (deposition rate is zero), and
C_{eq} is the equilibrium cohesive sediment concentration consisting of relatively weak flocks that are broken apart before reaching the bed or eroded immediately after deposition.

Full deposition allows the concentration to reduce to zero and is appropriate for low shear areas such as floodplains. Partial deposition allows concentration to approach to an equilibrium value (C_{eq}) and is appropriate for high shear main channel areas. If $\tau_f = \tau_p$, only the first equation, i.e., the full deposition, is applied and C_{eq} is ignored. If $C_{eq} = 0$, the first two equations collapse into one and it is meaningless to separate full and partial deposition modes. Under such scenarios, only the partial mode critical shear stress is used. Note that the first equation was due to Krone (1962) and the second equation was due to van Rijn (1993).

Many experiments were preformed to determine the full deposition critical shear stress. There was quite a scatter and it may range from 0.06 to 1.1 Pa. As an example, Krone (1962) conducted a series of flume experiments for the San Francisco Bay sediment. He found that $\tau_f = 0.06\ Pa$ when $C_k < 0.3\frac{kg}{m^3}$ and $\tau_f = 0.078\ Pa$ when $0.3 < C_k < 10\ kg/m^3$. Mehta and Partheniades (1973) found that $\tau_f = 0.15\ Pa$ for kaolinite in distilled water. In general, appropriate values of τ_f, τ_p and C_{eq} are not well understood. Thus, they should be either determined through laboratory and field measurements, or through calibration. As a reference, in the study of the erosion upstream of the San Acacia Dam on the Rio Grande River (Lai and Bauer, 2007), the laboratory measured data were determined to be $\tau_f = 0.005\frac{lb}{ft^2}$, $\tau_p = 0.021\frac{lb}{ft^2}$ and $C_{eq} = 1.0\frac{kg}{m^3}$. In modeling the Cheery Creek pressure flushing, erosion is the dominant process and deposition is not important, and therefore results are not sensitive to the choice of deposition rate formulation.

2.3. Bed Dynamics

Bed dynamics refers to how sediments in the bed interact with those in the water column. On one hand, sediment movement in the river modifies the bed topography and the sediment contents on the bed. On the other hand, the flow and sediments in the water column are altered due to bedform changes. Therefore, modeling of the bed dynamics is an integral part of alluvial modeling.

Bed sediments may be divided into an active layer and a number of subsurface layers. The volume or mass fractions of sediments within each layer, i.e., the bed gradation, are inputs at the beginning of the modeling and may change during bed evolution. It may be shown that the volume and mass fractions are equivalent if the specific gravity is the same for all sediment size classes (this is assumed in our study).

The elevation of bed surface (z_b) is changing due to net erosion and deposition. Change in bed elevation is contributed from all sediment size classes. The change in z_b due to sediment size class k is governed by the following equation:

$$\eta_{ak} \left(\frac{\partial Z_b}{\partial t} \right)_k = -\dot{V}_k = -\frac{1}{L}(p_k q_{bk}^* - q_{bk})$$

Where:

$\eta_{ak} = 1 - \sigma_{ak}$ is the porosity parameter,

σ_{ak} is the porosity for the k-th size class in the active layer,

$\dot{V}_k$ is the net volumetric erosion rate per unit bed area (or net rate of eroded depth) for size class k.,

q_{bk} is the bedload flux per unit width,
and q_{bk}^* is the equilibrium capacity of q_{bk}.

Note that $\dot{V}_k$ is computed from the net exchange rate. The above equation provides the net erosion and deposition of the sediments which would alter the sediment contents in the active layer. The value of porosity for natural systems range from 0.25 to 0.55 (Parker, 2006); a typical good value for spherical grains is 0.36 as given by random close packing.

In this study, the active layer is defined to be the top bed layer participating in the sediment exchange between water column and alluvial bed, while subsurface layers provide sediments to or receive sediments from the active layer. The thickness of the active layer is a user input. A constant thickness may be reasonably used. As reviewed by Merkel and Kopmann (2012), the selection of active layer thickness is empirical at present and inconclusive. A number of formulas for the active layer thickness was also discussed by Malcherek (2007).

The volume fraction of each sediment size class and the porosity of the active layer and subsurface layers are chosen as the two primitive variables. The governing equations for the two are needed within each bed layer. In our approach, the mass conservation equation is used to determine the volume fraction of sediment class in the active layer; it can be written as:

$$\frac{\partial m_a p_{ak}}{\partial t} = -\dot{V}_k + p_{2k} \sum_i \dot{V}_i \qquad \text{if net erosion } (\sum_i \dot{V}_i \geq 0)$$

$$\frac{\partial m_a p_{ak}}{\partial t} = -\dot{V}_k + p_{ak} \sum_i \dot{V}_i \qquad \text{if net deposition } (\sum_i \dot{V}_i < 0)$$

Where:

m_a is the total volume per unit area without void (or mass) of sediments in the active layer,

p_{ak} is the volume fraction of k-th class in the active layer ($\sum_k p_{ak} = 1$),

p_{2k} is the volume fraction of k-th class in the first subsurface layer (beneath the active layer).

In the modeling the total volume (or mass) per unit area (m_a) remains constant throughout the simulation, while the thickness of the active layer may change.

The m_a value is computed at the beginning of the computation based on the thickness of the active layer (δ_a). The thickness, δ_a, is a function of flow and sediment conditions as well as the bedform evolution. But δ_a can also be a user supplied parameter. By default, δ_a is set as $N_a d_{90}$ with N_a ranging from 1.0 for large boulders to more than 14.0 for fine sediments.

The porosity of the active layer is governed by the volume conservation equation derived from the kinematic constraint and may be expressed as:

$$\frac{\partial \delta_{ak}}{\partial t} = -\frac{\dot{V}_k}{\tilde{\eta}_k} + p_{2k} \frac{\sum_i \dot{V}_i}{\eta_{2k}} \qquad \text{if } \sum_i \dot{V}_i \geq 0$$

$$\frac{\partial \delta_{ak}}{\partial t} = -\frac{\dot{V}_k}{\tilde{\eta}_k} + p_{ak} \frac{\sum_i \dot{V}_i}{\eta_{ak}} \qquad \text{if } \sum_i \dot{V}_i < 0$$

Where:

δ_{ak} is the volume per unit area for size k of the active layer thickness including voids; relation between δ_{ak} and η_{ak}: $\delta_{ak}\eta_{ak} = p_{ak}m_a$.

In the above, $\tilde{\eta}_k$ is computed as:

$\tilde{\eta}_k = \eta_{ak}$ if $\dot{V}_k \geq 0$ (k-th size is eroded from active layer)

$\tilde{\eta}_k = \eta_{sk}$ if $\dot{V}_k < 0$ (k-th size is deposited into active layer)

and η_{sk} is the porosity parameter for the suspended sediment. The above equations may be more conveniently written as:

$$\frac{\partial \delta_{ak}}{\partial t} = -\frac{\dot{V}_k}{m_a p_{ak}}\delta_{ak} + p_{2k}\frac{\sum_i \dot{V}_i}{\eta_{2k}} \qquad \text{if } \sum_i \dot{V}_i \geq 0 \text{ and } \dot{V}_k \geq 0$$

$$\frac{\partial \delta_{ak}}{\partial t} = -\frac{\dot{V}_k}{\eta_{sk}} + p_{2k}\frac{\sum_i \dot{V}_i}{\eta_{2k}} \qquad \text{if } \sum_i \dot{V}_i \geq 0 \text{ and } \dot{V}_k < 0$$

$$\frac{\partial \delta_{ak}}{\partial t} = \frac{p_{ak}\sum_i \dot{V}_i - \dot{V}_k}{m_a p_{ak}}\delta_{ak} \qquad \text{if } \sum_i \dot{V}_i < 0 \text{ and } \dot{V}_k \geq 0$$

$$\frac{\partial \delta_{ak}}{\partial t} = -\frac{\dot{V}_k}{\eta_{sk}} + \frac{\sum_i \dot{V}_i}{m_a}\delta_{ak} \qquad \text{if } \sum_i \dot{V}_i < 0 \text{ and } \dot{V}_k < 0$$

The volume fraction (p_{Lk}), the porosity parameter (η_{Lk}), and the thickness (t_L) of subsurface layers are also updated. In the model, the subsurface layer underneath the active layer ($L = 2$) exchanges sediments with the active layer so that the mass of each size class is maintained in the active layer. In the process, the thickness of layer 2 may increase or decrease. The remaining subsurface layer remains unchanged until the thickness of layer 2 is reduced to zero. Under such a circumstance, layer 3 replaces layer 2 and the total number of subsurface layers is reduced by one at the point. For layer 2, the volume fraction (p_{2k}), the porosity parameter (η_{2k}), and its thickness are computed. If net erosion occurs ($\sum_i \dot{V}_i \geq 0$), p_{2k} and η_{2k} do not change, and the thickness change is governed by:

$$\frac{dt_{2k}}{dt} = -\left(\sum_i \dot{V}_i\right)\left(\sum_i \frac{p_{2i}}{\eta_{2i}}\right)$$

where subscript *i* runs through all sediment size classes. If net deposition occurs ($\sum_i \dot{V}_i < 0$), the thickness change is governed by:

$$\frac{dt_{2k}}{dt} = -\left(\sum_i \dot{V}_i\right)\left(\sum_i \frac{p_{ai}}{\eta_{ai}}\right)$$

and p_{2k} and η_{2k} are modified by fully mixing the new depositions from the active layer with the sediments already in layer 2.

2.4. About 3D Mesh

A special 3D mesh is adopted with U^{2}RANS, called the unstructured physical coordinate (UPC) sigma mesh. Briefly, a UPC sigma mesh adopts unstructured polygonal cells in the horizontal plane and an equal number of mesh points in the vertical direction. With the UPC mesh, all 3D coordinates are in the physical coordinates and no transformation of the governing partial differential equations are carried out. Key differences between the UPC sigma mesh and the traditional sigma mesh are:

- Horizontal mesh uses arbitrary polygons (a mesh with hybrid quadrilaterals and triangles is a special case);

- Physical coordinates are used spatially so that the original and simple governing equations expressed in the Cartesian coordinate system are discretized and solved; and

- Vertical mesh points are physical and may be moved to conform to the moving boundaries in a simple manner and redistributed easily.

With the proposed UPC sigma mesh, a flexible 2D mesh may be generated first using a 2D mesh generator (this has been routinely carried out by engineers for practical projects). A 3D mesh may then be generated automatically based on the known bed elevation and free surface elevation (Only a vertical number of points need to be specified). The UPC mesh module requires no sophisticated 3D mesh generator but has certain limitations. The two major constrains are:

- It is difficult to represent an object into the model domain with the UPC mesh since all geometry has to be represented by the initial 2D mesh; and

- Very fine and distorted mesh cells may be generated in steep and shallow areas.

For a more detailed descriptions and demonstrations of the UPC sigma mesh, refer to the report by Lai (2017).

3. Model Demonstration and Application

The 3D numerical model, U^{2}RANS, is applied to simulate the pressure flushing process of the Cherry Creek Reservoir, Denver, Colorado. Model setup details and simulated results are documented below.

3.1. Mesh Generation

A 3D mesh is necessary for the numerical modeling and the process is described below.

First, the horizontal model domain is determined as shown in Figure 1. The determination process is as follows. First, the boundary of the wetted reservoir is obtained based on the available 2017 pre-flushing of Geographic Information System (GIS) raster data and the water surface elevation (WSE). The terrain contour line 5,550 feet is used to represent the reservoir boundary since WSE is about 5,550 feet during the pressure flushing (See Figure 2). Second, a portion of the wetted reservoir near the intake is selected for simulation, as only the area near the intake has significant flows and is important for the pressure flushing process. Third, the intake itself is added to the model domain—the rectangle in the figure with a horizontal dimension of 69 feet wide and 40 feet deep (Figure 3 and Figure 4). The intake trash rack and gate opening dimensions are shown in Figure 3, Figure 4, and Figure 5. Fourth and final, the five gates are extended out so that water release amounts may be implemented properly using the numerical boundary conditions. Without the extension, boundary condition has to be applied right at the gate openings which may lead to heightened uncertainty of simulated results.
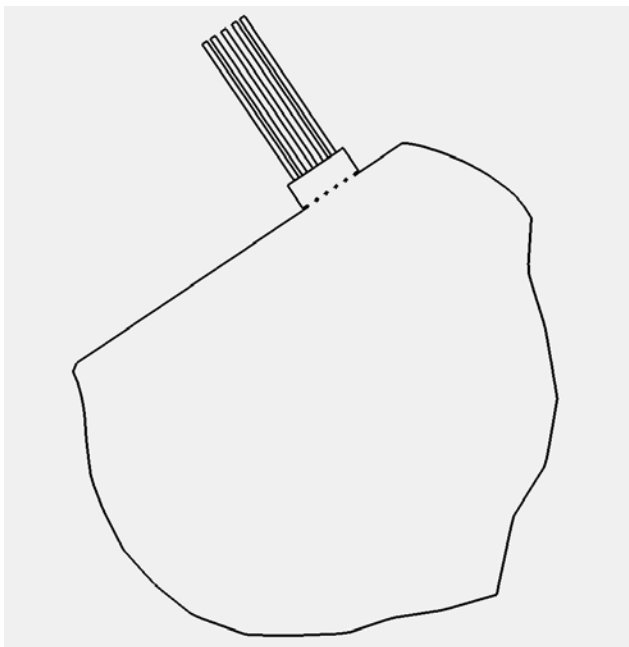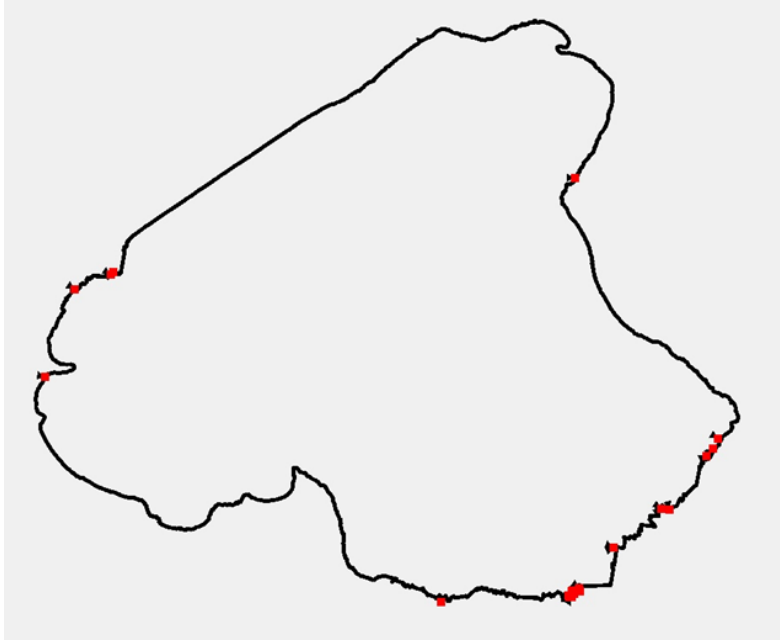

Figure 1. Model domain selected.

Figure 2. The reservoir boundary based on the 5550 feet terrain elevation line.
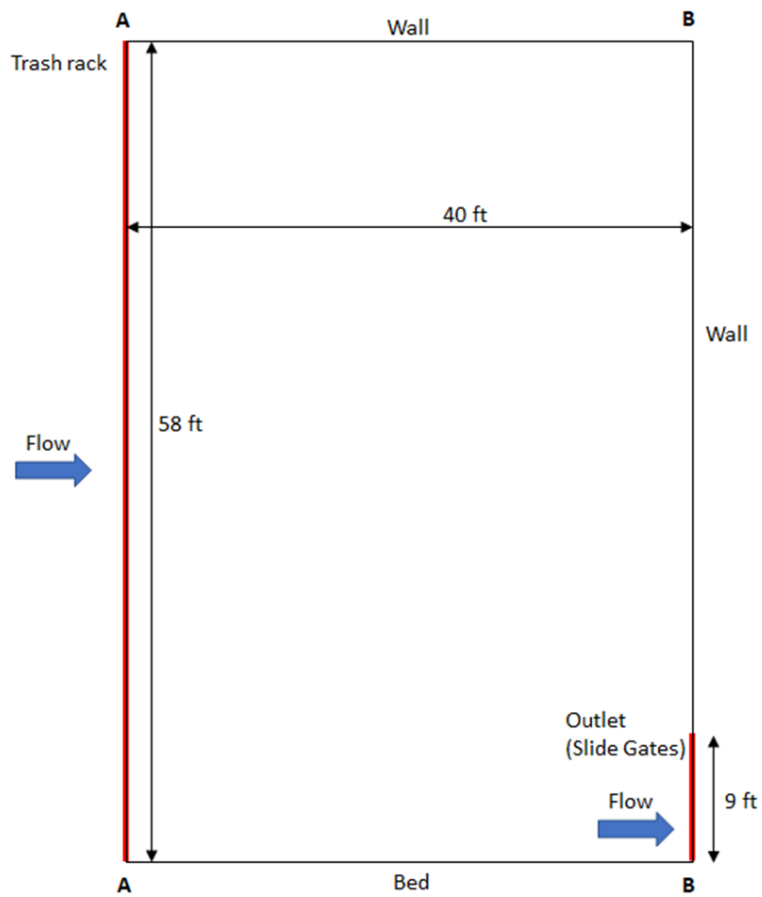
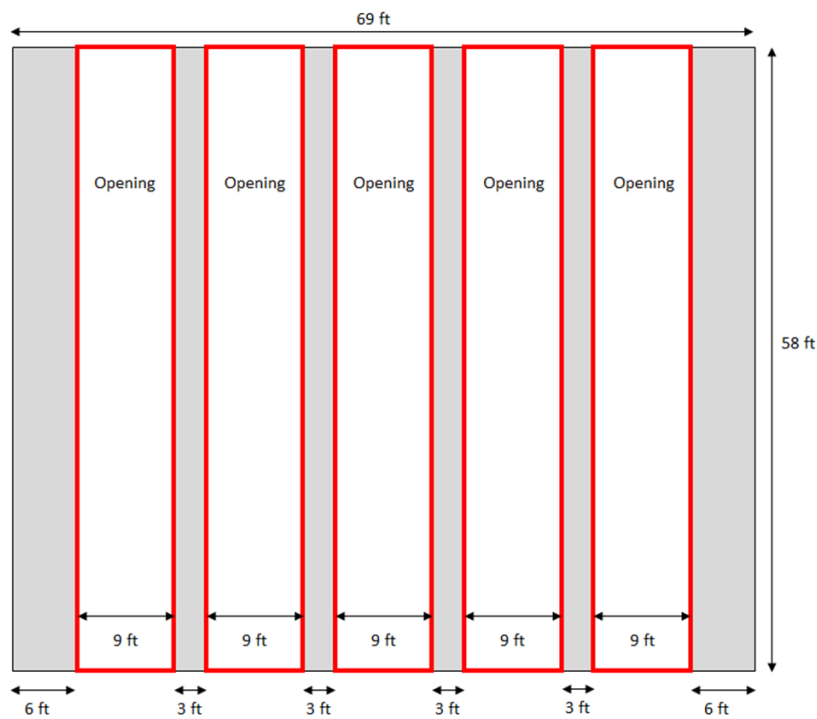Figure 3. Side view of the intake with intake tower dimensions.

Figure 4. Front view of the intake with trash rack dimensions.
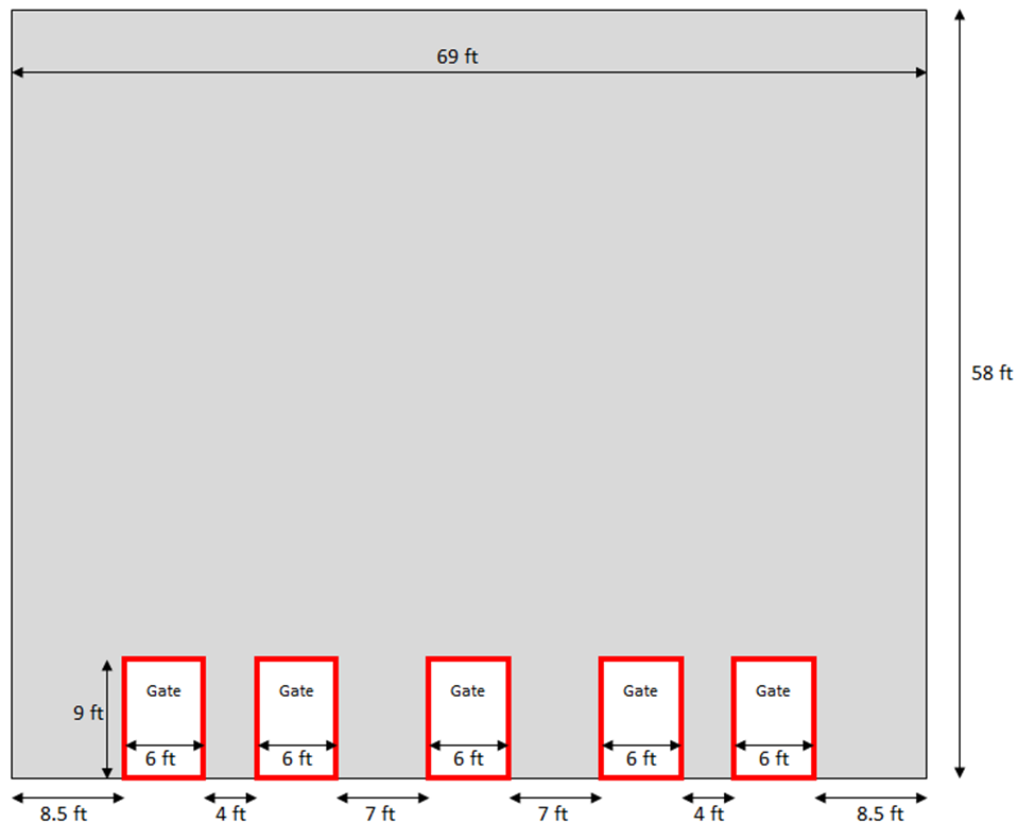
Figure 5. Front view of the intake back wall with five gate opening dimensions.

Next, a 2D mesh is generated covering the horizontal model domain (Aquaveo's Surface Water Modeling System, SMS, is used). The final 2D mesh adopted is shown in Figure 6 and Figure 7. Once the 2D mesh is obtained, the bed elevation (terrain) is interpolated onto the mesh and is also displayed in the figures. The terrain data, Figure 8, is based on the boat survey carried out by the TSC (Dombroski, 2018 and Collins et al., 2019) right before the 2018 pressure flush. The bed elevation within the intake is to be discussed later. The 2D horizontal mesh consists of 9,855 mixed quadrilaterals and triangles.
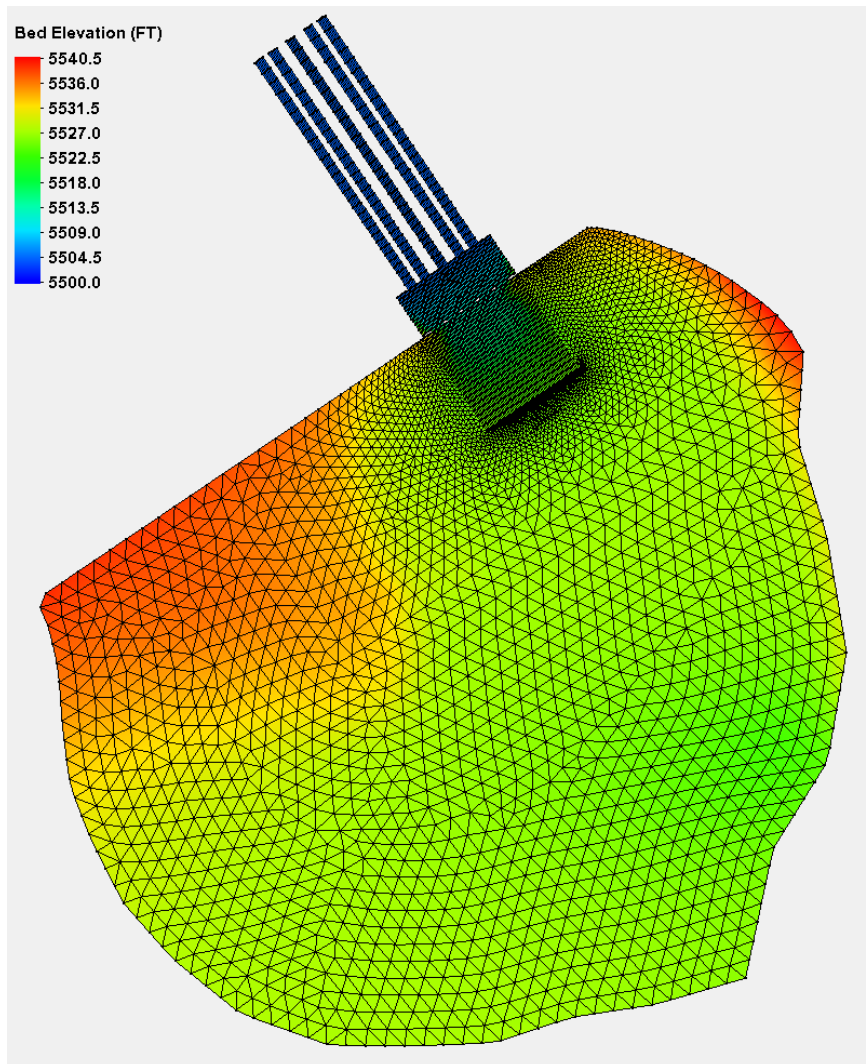

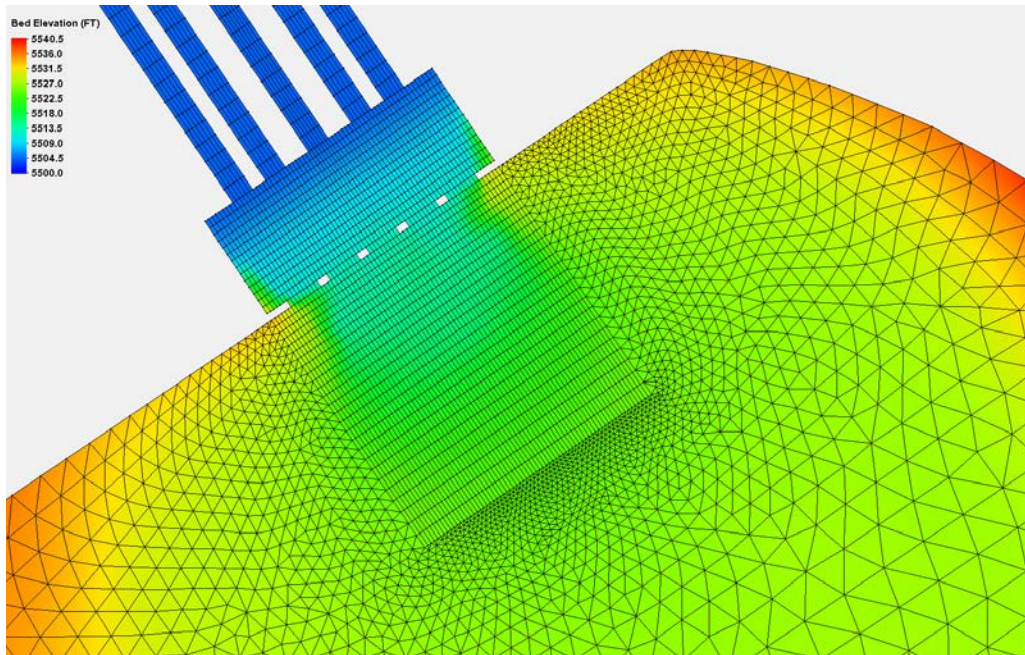Figure 6. 2D mesh covering the horizontal model domain, along with the terrain data representing the bed elevation.

Figure 7. Zoom-in view of the horizontal mesh in the intake area.
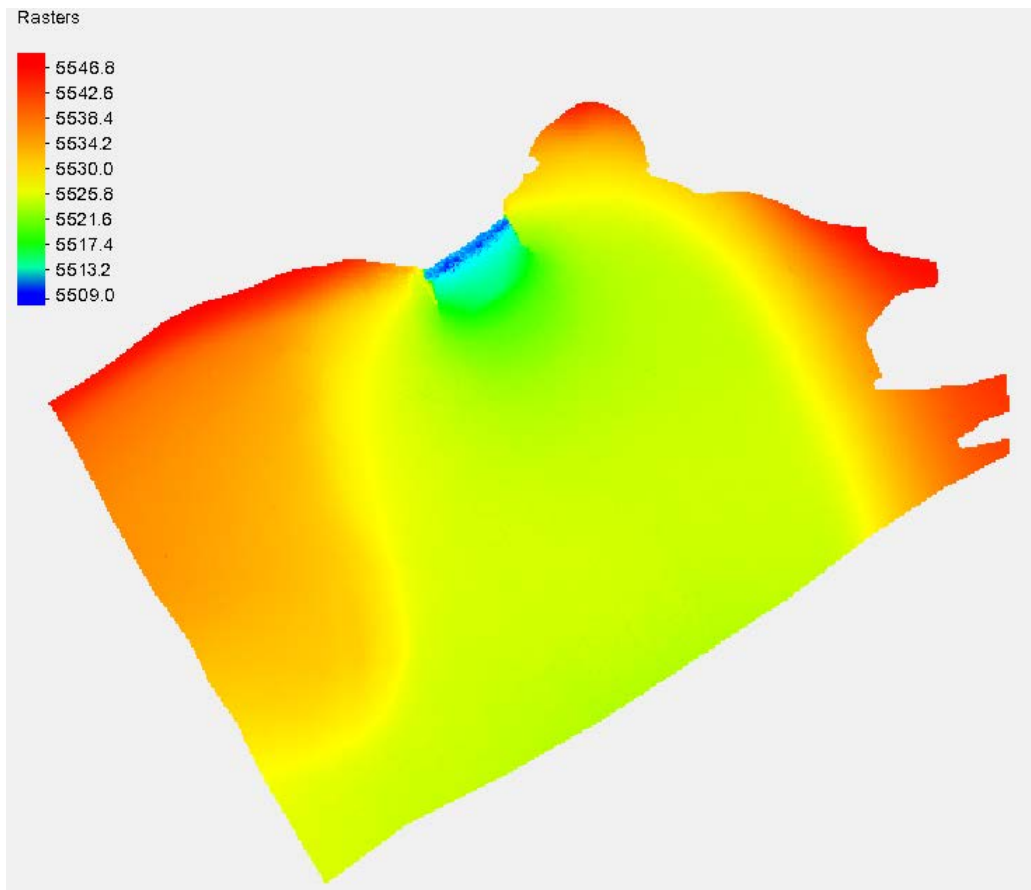
Figure 8. Pre-2018 bed elevation based on the boat reservoir survey.

Finally, the 3D mesh is generated automatically by U^{2}RANS using the sigma-mesh technique. That is, the same number of vertical mesh points are used at each 2D mesh point between the bed elevation and the water surface. In the simulation, a total of 47 uniform points are used so that the vertical mesh size is about 1 foot in the deepest area between 5504 feet and 5550 feet. A view of the final 3D mesh is shown in Figure 9.
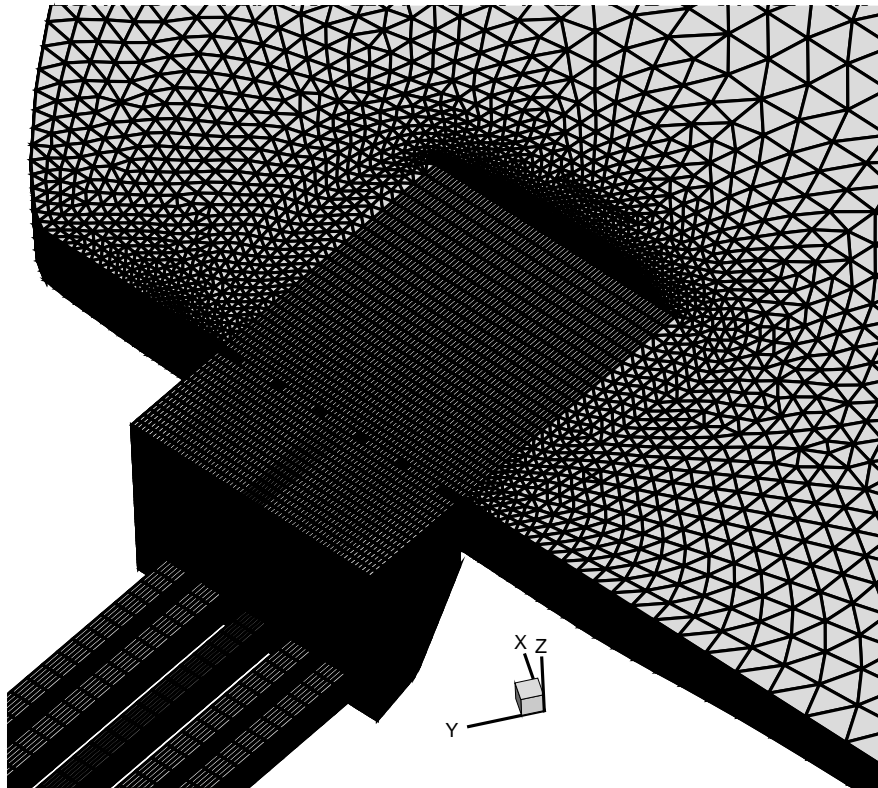

Figure 9. Close-up view of the 3D mesh near the intake.

3.2. Model Inputs

Two sets of modeling were carried out corresponding to two pressure flushing operations at the Cheery Creek Reservoir: 2017 low-discharge and 2018 high-discharge flushing. The flushing release rates are inputs to the model as the boundary conditions, while other model parameters (to be discussed below) remained the same for all modeling runs unless it is explicitly mentioned in the report.

The 2017 flushing was conducted on May 24, 2017 with a nominal discharge of 250 cfs. The actual flow release through the intake gates is shown in Figure 10. The release was through one of five gates and follows the gate sequence of 3, 1, 2, 4, 5 when the gates are numbered from right to left looking towards the intake. The 2018 flushing took place on May 23, 2018 with a nominal discharge of 1,300 cfs. The actual release flow is in Figure 11. Again, only one gate was opened for the release and the sequence of gate opening is the same as the 2017 release.
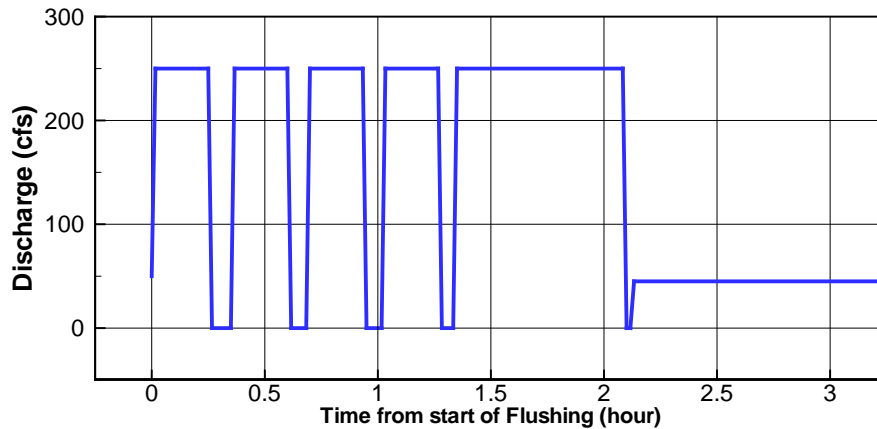
Figure 10. Actual 2017 flow release rate through the five gates of the intake.
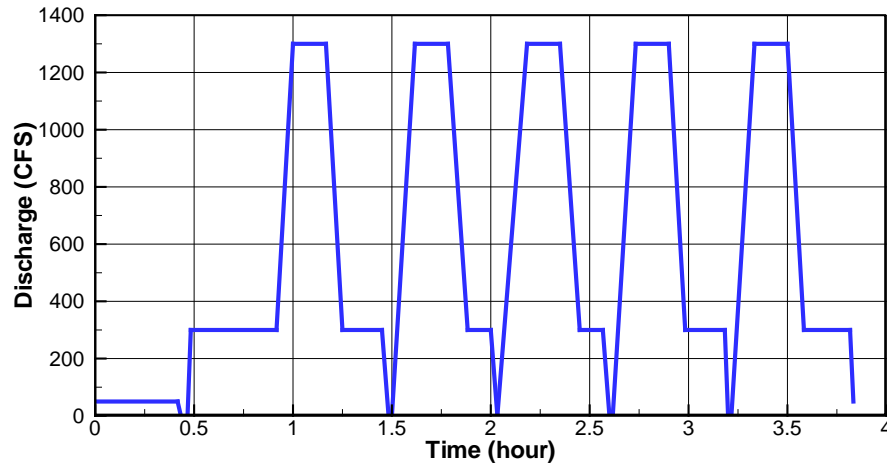

Figure 11. Actual 2018 flow release rate.

The remaining inputs are the same for both 2017 and 2018 releases and they are as follows.

The sediments in the Cheery Creek Reservoir consists of clay, silt, and sand. According to Armstrong (2017), the diameters of clay, silt, and sand are less than 0.002 millimeters (mm), between 0.002 mm and 0.075 mm, and above 0.075 mm. Based on the bed gradations in the near-surface samples (see Table 1), the fractions for clay, silt and sand are 45%, 50%, and 5%, respectively. In this study, therefore, one cohesive sediment class is selected for the modeling, as about 95% of the sediments are in the clay and silt sizes. According to Armstrong (2017), the average of measured surface sediment specific density was about 2.51; the bulk density was 32.5 pounds per cubic foot (lb/ft^3) (520.6 kilograms per cubic meters [kg/m^3]).

Table 1. Sediment Gradation Results for the Near-Surface Samples (Armstrong, 2017).

Sample Number	Depth (ft)	Clay (%)	Silt (%)	Sand (%)
DH-17-2-1	0.0	47.7	49.4	2.9
DH-17-3-1	1.1	61.9	37.1	1
DH-17-4-1	0.3	28.9	61.3	9.8
Average	-	45	50	5

The most important inputs are related to the sediment thickness distribution and its erodible properties. The sediment thickness distribution is an important input; the model domain is partitioned into three zones (Figure 12) for the purpose: the reservoir (red), the intake upstream of the gates (gray), and the after-gates (green). The thickness in the reservoir is large according to the survey, and the erosion in the area is almost negligible—so 5-meter thickness is the input which does not impact the results. The after-gate area is specified as having no sediments deposited and non-erodible during the simulation. The sediment thickness of the intake (gray) zone is the most important for the present simulation; unfortunately, no measured data are available. The baseline thickness input in the intake is set up as follows. The thickness at the trash rack is obtained by averaging the measured bed elevation in the area and subtracting out the intake elevation of 5,504 feet. This showed that about eight (8) feet of sediments were deposited near the trash rack and is taken as the thickness. This thickness is assumed to be constant inside the intake except near the gates. A linear drop of thickness from 8 to 0 feet is assumed near the gate over a 4-fot distance. The baseline bed elevation (thickness) distribution in the intake and its vicinity are displayed in Figure 13. Due to the importance of the intake sediment thickness, sensitivity study will be reported later by varying the thickness different from the baseline.
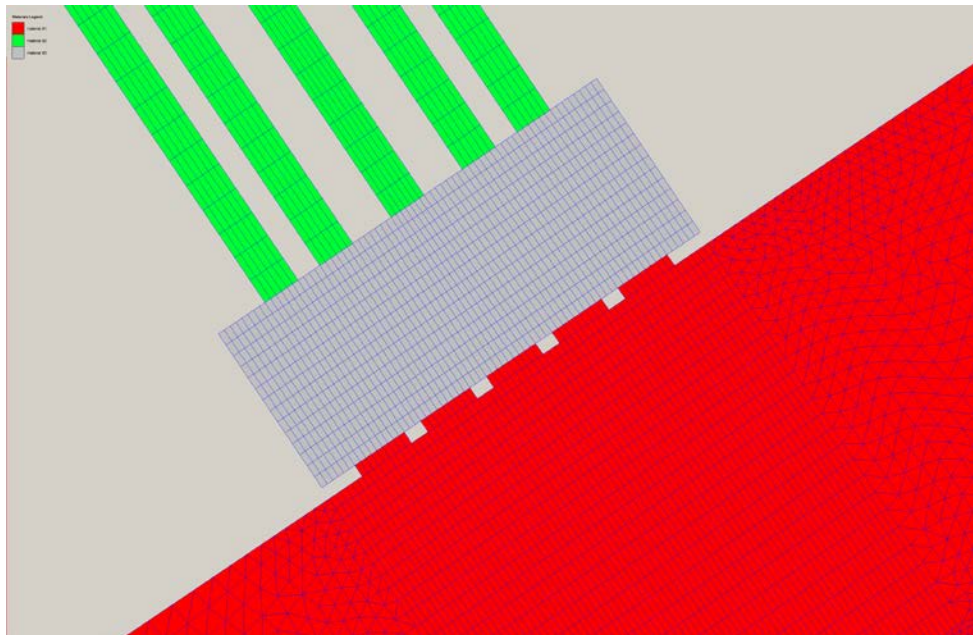

Figure 12. Three spatial zones are used to specify the sediment thickness distribution.

Thickness (ft)

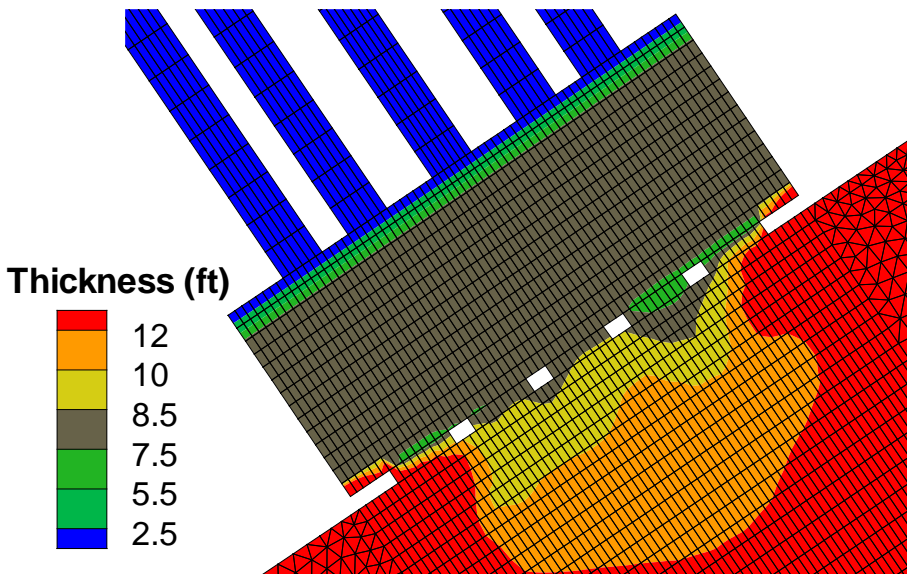|	
🟥	12
🟧	10
🟨	8.5
⬛	7.5
🟩	5.5
🟩	5.5
🟦	2.5

Figure 13. Thickness of the erosible sediments inside the intake (thickness is about 8 feet in the intake).

The next important input is the erodibility properties of the sediment. In the present modeling, constant critical shear stress and erodibility are specified as inputs. The two parameters are based on the JET test results of Armstrong (2017). The test showed that the critical shear stress and erodibility (detachment rate) varied widely at different locations (see Table 2). The measured data at the DH-17-2-1 were used in the present study as it is closer to the intake. That is, the critical shear stress is 0.013 psf (0.62 Pa) and the erodibility/detachment rate is 200.6 ft/hr-psf (3.547e-4 m/s-Pa). The results are more sensitive to the erodibility than the critical shear stress; and some sensitivity results will be reported later in addition to the baseline setup.

In this study, the k-ε turbulence model is selected.

Table 2. JET Test Results of Critical Shear Stress (lb/ft^2 or psf) and Detachment Rate (ft/hr-psf) at Three Locations Near the Bed Surface (Armstrong, 2017).

Sample Number	Depth (ft)	Detachment Rate (ft/hr-psf)	Critical Shear Stress (psf)
DH-17-2-1	0.0	200.6	0.013
DH-17-3-1	1.1	3.64	0.048
DH-17-4-1	0.3	18.45	0.06
Average	-	74.2	0.04

3.3. 2017 Pressure Flush Results

The above baseline numerical model is used to simulate the 2017 pressure flushing process. The model results are presented and discussed next.

First, the simulated sediment concentration during the flushing is compared with the only available field data. Note that the numerical model concentration is obtained right after the gates (within the outlet works), while the measured sediment concentration is within the Cherry Creek at the small golf cart bridge about 0.5 mile downstream of the dam outlet (see Figure 14 and Dombroski, 2018). Cherry Creek flows through the golf course and continues to its confluence with the South Platte River, approximately 12 miles downstream of the dam.

The measured and simulated sediment concentration is compared in Figure 15. It is seen that the numerical model over-predicts the concentration significantly. The chief causes include:

- The unknown sediment thickness immediately upstream of the intake gates.
- High uncertainty of the sediment erodibility.
- Numerical results are not at the same location as the measured ones.

Figure 14. Aerial imagery of site with indication of 2017 and 2018 sediment sampling locations (Source: Dombroski, 2018).
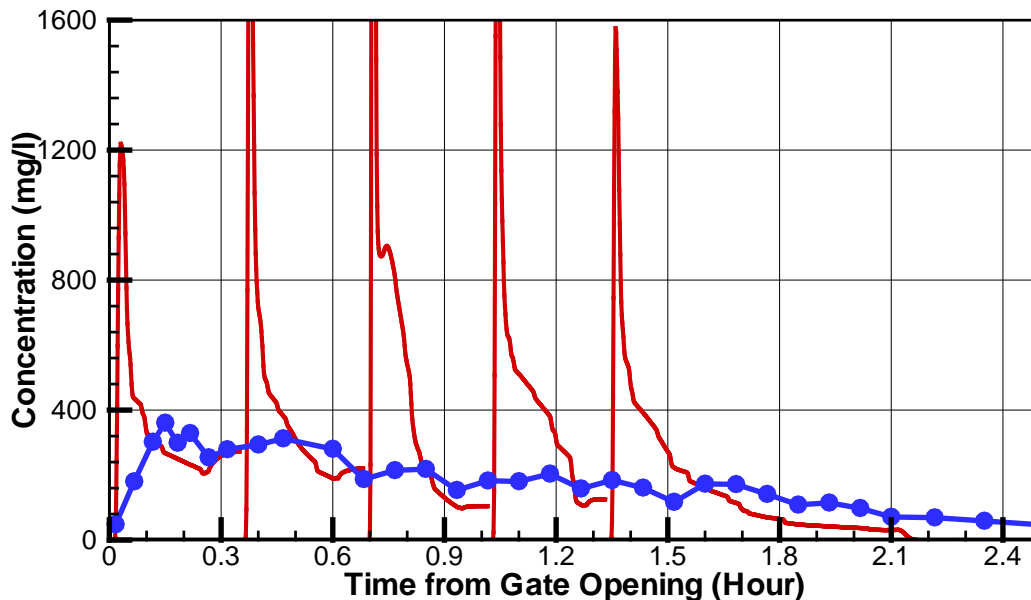
Figure 15. Baseline model predicted and field measured sediment concentration downstream of the release gate during the 2017 pressure flushing (Red line: numerical model; blue symbol and line: measurement). Concentrations are in milligrams per liter (mg/L).

The computed concentration has clear high peaks which are not observed in the field. This may be explained by the fact that the measured location is 0.5 mile downstream of the outlet and sediment concentration has been "well-mixed." The total amount of sediment is over-predicted by the baseline model, which may be due to the unknow sediment thickness in the intake.

A number of sensitivity runs are carried out in order to understand the model results.

First, sensitivity to the sediment thickness within the intake is carried out. An additional thickness input is created, which has less sediments (smaller thickness) near the gates than the baseline. The new thickness is shown in Figure 16 which is the same as the baseline except that the thickness is linearly reduced from 8 to 0 feet over a 8-foot distance (versus the 4-foot distance with the baseline). The model is re-run with everything else are kept the same. The simulated release sediment concentration is compared with the measured data in Figure 17. It is seen that the predicted concentration peak is much reduced in comparison with the baseline model.
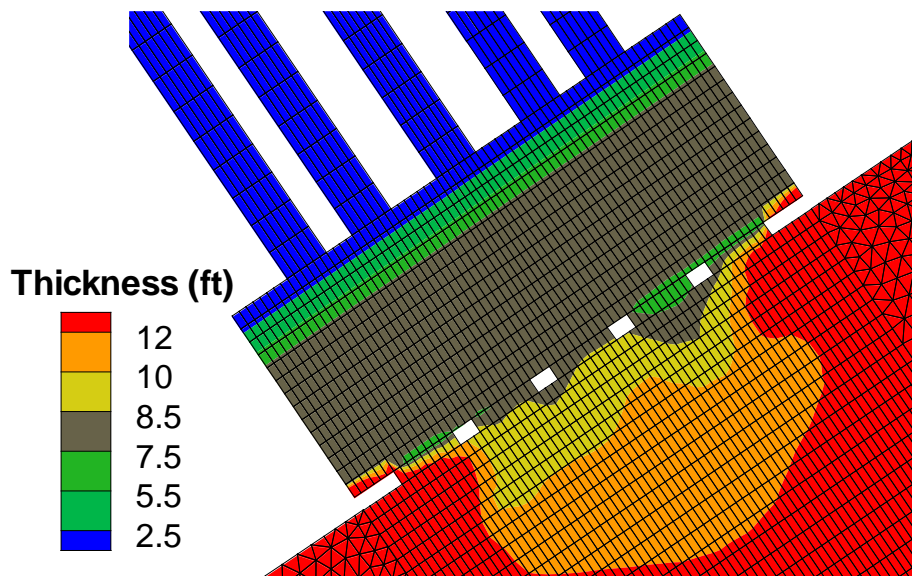
Figure 16. Thickness of the erosible sediments inside the intake with the sensitivity study.
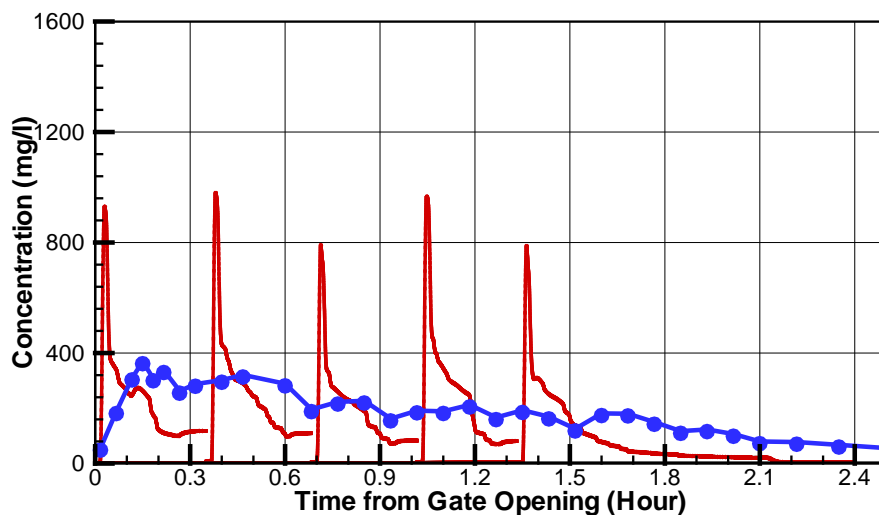

Figure 17. Sensitivity to the sediment thickness of the sediment concentration downstream of the release gate during the 2017 pressure flushing (Red line: numerical model; blue symbol and line: measurement).

Another sensitivity run is carried out by reducing the erodibility from the baseline value of 3.547e-4 m/s-Pa to 1.0e-4 m/s-Pa. The simulated release concentration is compared with the measured data in Figure 18. The concentration peak is drastically reduced only during the first gate opening, but not the other four gates. Overall, the total amount of sediment is reduced. The sensitivity study showed that erodibility is an important parameter, but less important than the sediment thickness.
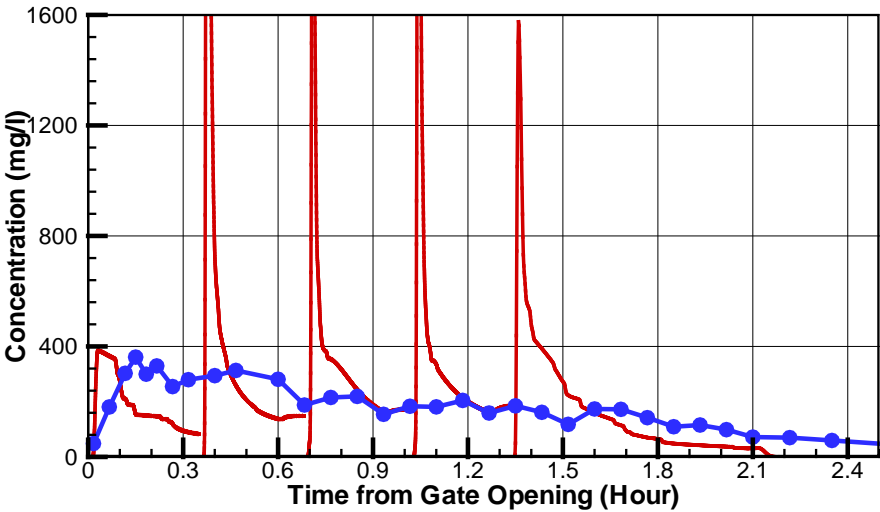
Figure 18. Sensitivity to erodibility of the sediment concentration downstream of the release gate during the 2017 pressure flushing (Red line: numerical model; blue symbol and line: measurement).

It is more interesting to learn the erosion pattern produced by the pressure flushing; and the scour zone is shown in Figure 19. The numerical modeling shows that the scour zone is limited to near-gate areas and within the intake. This is qualitatively confirmed by the fact that both the 2017 and 2018 field measurements in the reservoir were unable to detect measurable scours upstream of the trash rack in the reservoir. Quantitative comparison, however, is not possible as the field measurements were not able to reach inside the intake.
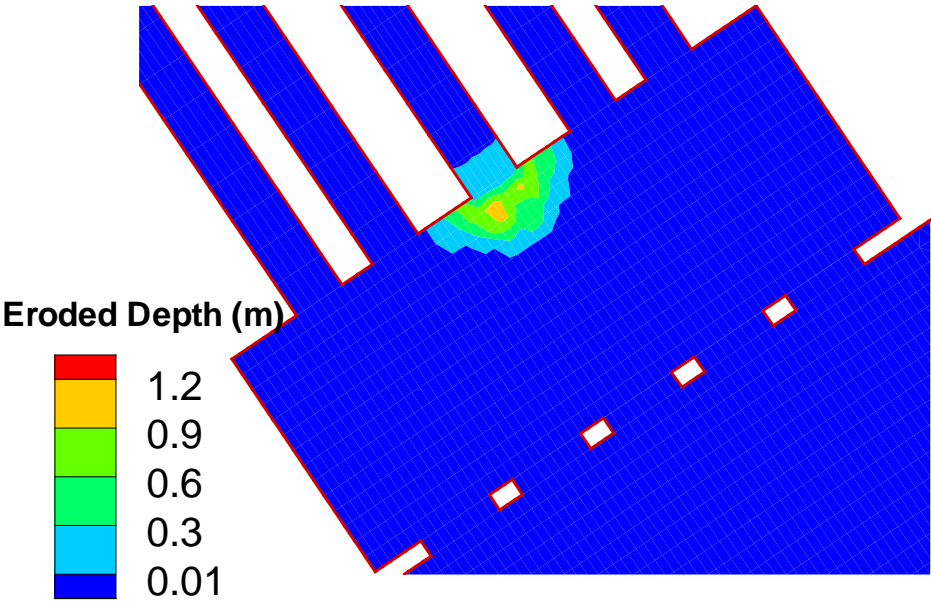
(a)   Time = 0.32 Hour (after Gate 3 release is complete)

Eroded Depth (m)

■ (red)	1.2
■ (orange)	0.9
■ (green)	0.6
■ (cyan)	0.3
■ (blue)	0.01
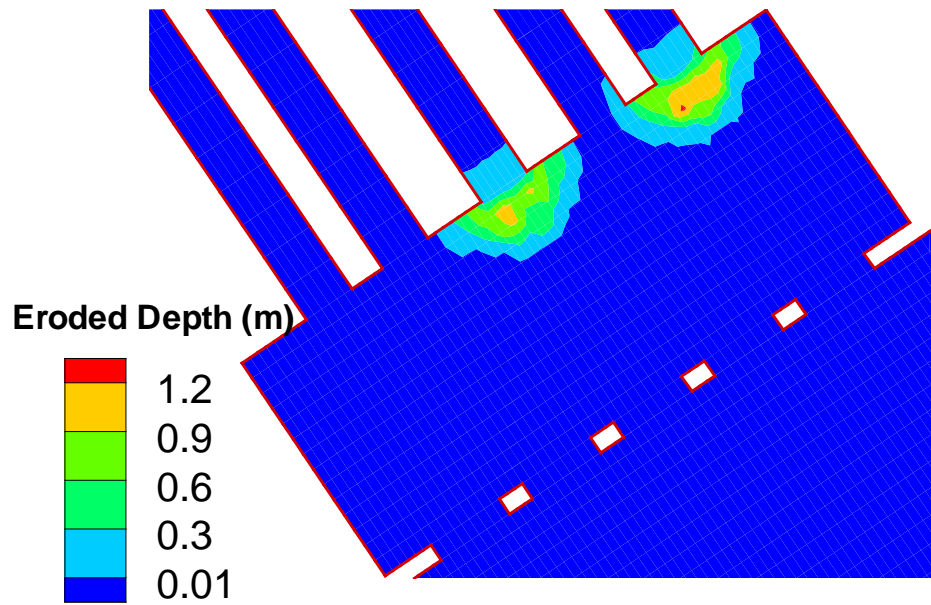
(b)   Time = 0.64 hour (after Gate 1 release is complete)

Eroded Depth (m)

■ (red)	1.2
■ (orange)	0.9
■ (green)	0.6
■ (cyan)	0.3
■ (blue)	0.01
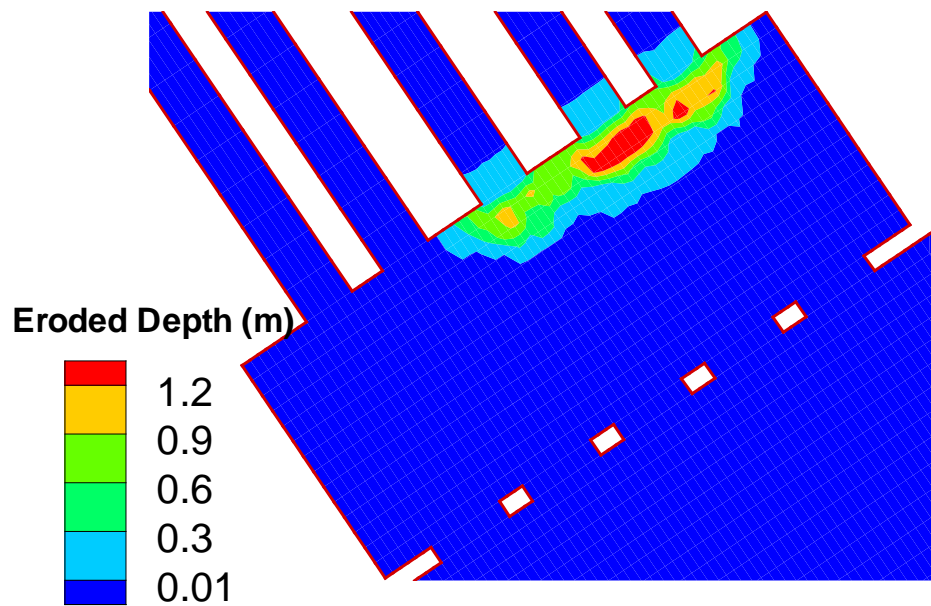
(c)   Time = 0.96 Hour (after Gate 2 release is complete)
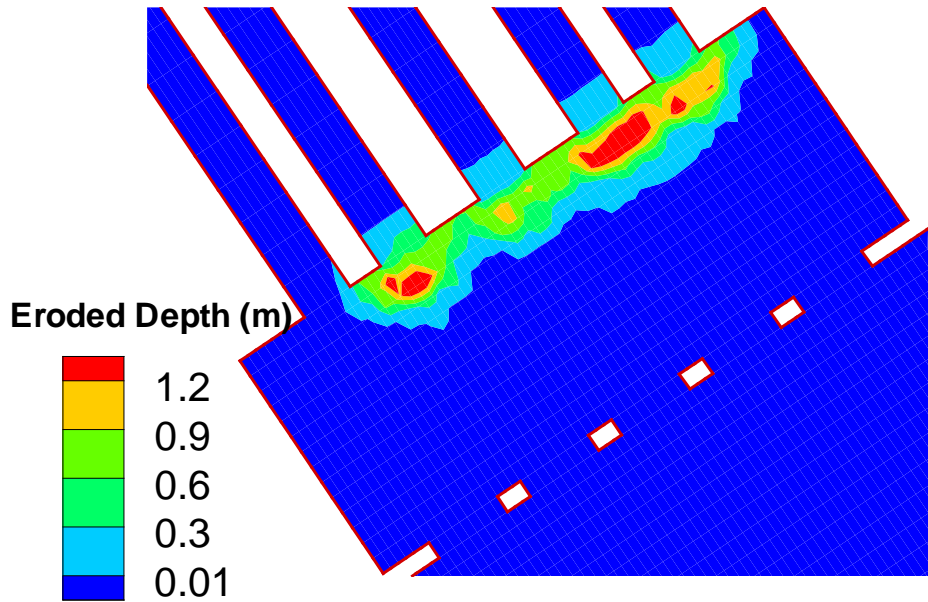
(d)   Time = 1.28 Hour (after Gate 4 release is complete)
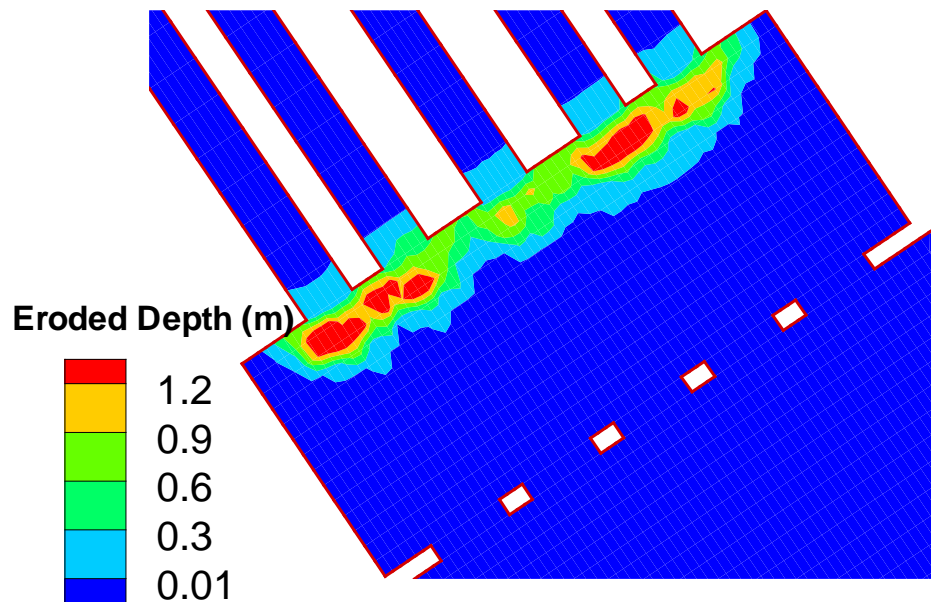
(e) Time = 2.4 hour (end of flushing)

Figure 19. Predicted scour zone development in time by the baseline model during the 2017 flushing (contours represent the eroded depth in meters). Panels (a) through (e) are for simulations times 0.32 to 2.4 hrs.

3.4. 2018 Pressure Flush Results

The same baseline numerical model is also used to simulate the 2018 pressure flushing process which has a much higher release rate (1,300 cfs in 2018 compared to 250 cfs in 2017). The model results are presented and discussed next.

The simulated sediment concentration during the 2018 flushing is compared with the field data. Similar to the 2017 release, the numerical model concentration is obtained right after the gates, while the measured sediment concentration is within the Cherry Creek at another bridge about 0.25 mile downstream of the dam outlet (see Dombroski, 2018 and Figure 14). Note that the 2018 measurement location is 0.25 mile closer to the release outlet than 2017. This may partially explain why the 2018 data is less mixed and shows gate-to-gate peak variations.

The measured and simulated sediment concentration is compared in Figure 15. It is seen that the numerical model agrees with the data much better than the 2017 flushing event. Overall, the concentration is under-predicted over the first 2-gates period while it is over-predicted over the next 3-gates period. The total amount of sediment release is close to the measured data. It is possible that the initial measured high concentration is partially contributed by the sediments stored downstream of the release outlet, not entirely due to the reservoir release.

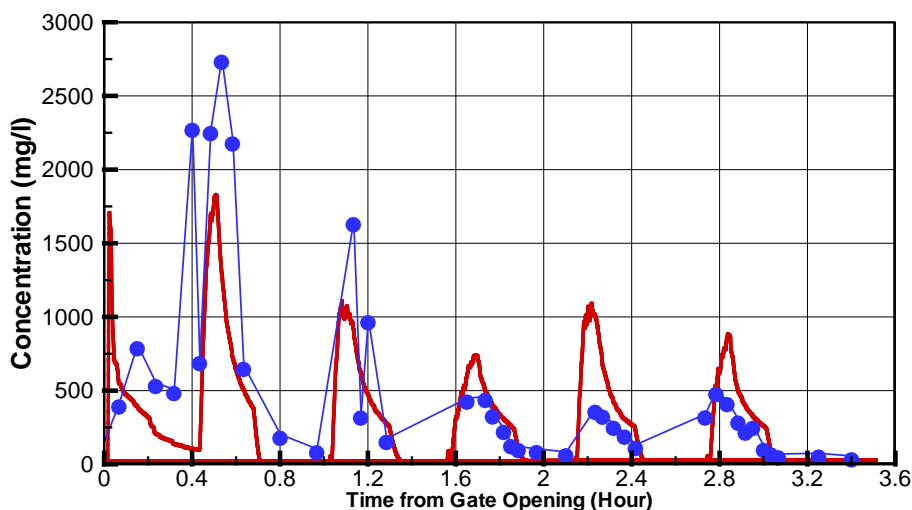Figure 20. Baseline model predicted and field measured sediment concentration downstream of the release gate during the 2018 pressure flushing (Red line: numerical model; blue symbol and line: measurement).

Similar to the 2017 modeling, a number of sensitivity runs are carried out as the model results are sensitive to the sediment thickness within the intake and erodibility. The sensitivity results are reported below.

Sensitivity to the sediment thickness within the intake is carried out. Two additional thickness inputs are created; they have less sediment (smaller thickness) near the gates than the baseline. The sensitivity thickness #1 is the same as that used in the 2017 modeling, as discussed in Figure 16. The thickness is decreased from 8 feet to 0 over an 8-foot distance. The sensitivity thickness #2 has even less thickness; its thickness is linearly reduced from 8 to 0 feet over the entire length of the intake (about 28 feet from the gate to the trash rake). Thickness #2 is displayed in Figure 21.

The model is re-run with both thickness options and other inputs remain the same. The simulated release sediment concentration is compared with the measured data in Figure 22. It is seen that the predicted concentration is decreased in comparison with the baseline model, demonstrating that the predicted sediment release is highly dependent on the available sediments in the intake.
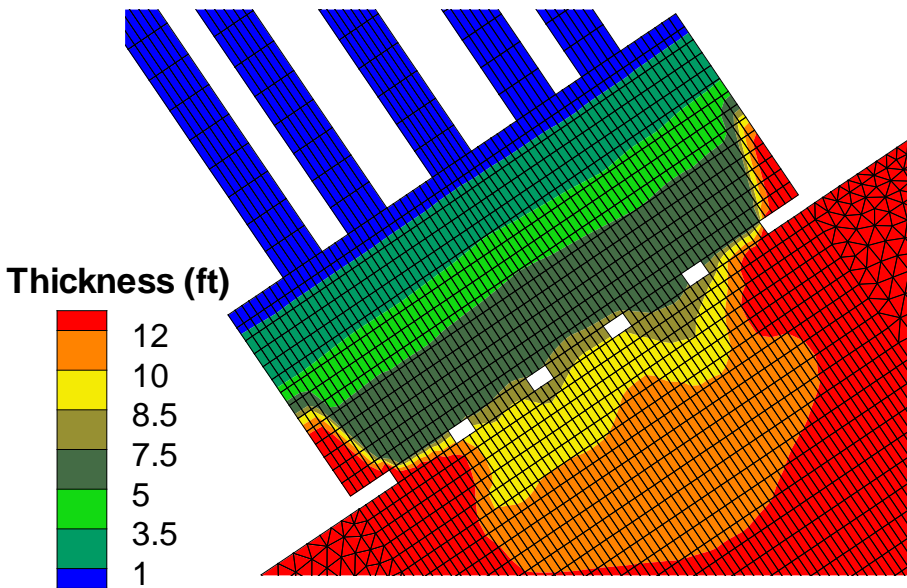
Figure 21. Thickness of the erodible sediments inside the intake with the sensitivity study.
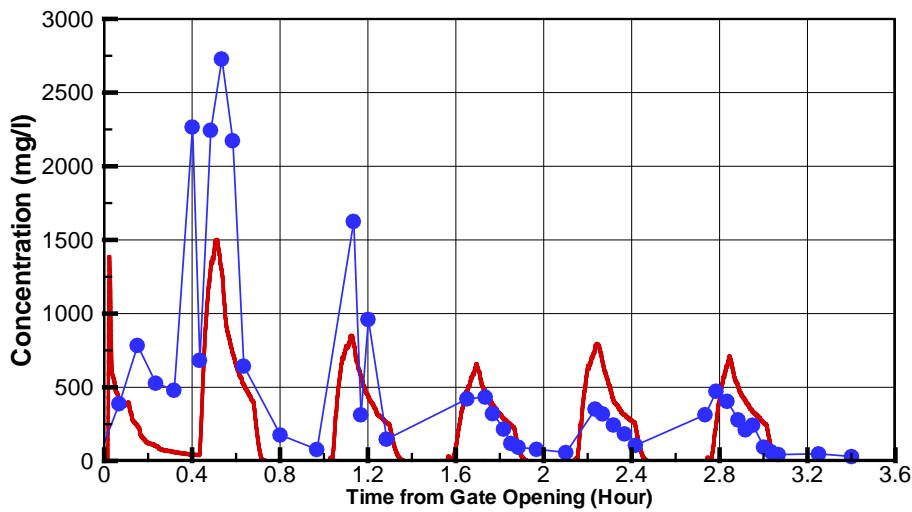
(a)   Thickness sensitivity #1
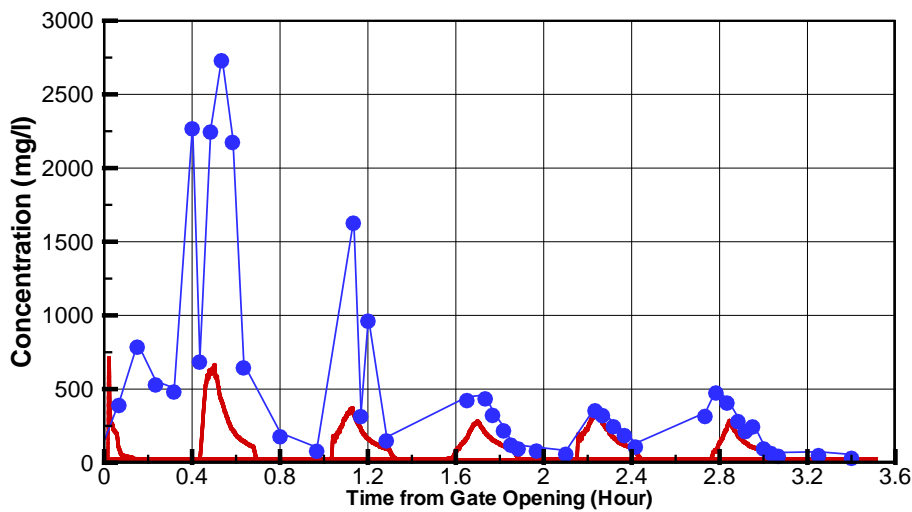
(b)   Thickness sensitivity #2

Figure 22. Sensitivity to the sediment thickness of the sediment concentration downstream of the release gate during the 2018 pressure flushing (Red line: numerical model; blue symbol and line: measurement).

Finally, the erosion pattern (scour zone) produced by the 2018 pressure flushing is shown in Figure 23. The numerical modeling shows that the scour zone is still limited to within the intake with the much higher 2018 release rate of 1,300 cfs. This is qualitatively confirmed by the fact that both the 2018 field measurements in the reservoir were unable to detect measurable scours upstream of the trash rack in the reservoir. Quantitative comparison, however, is not possible as the field measurements were not able to reach inside the intake.

Eroded Depth (m)

▮	2.4
▮	1.5
▮	0.8
▮	0.4
▮	0.01
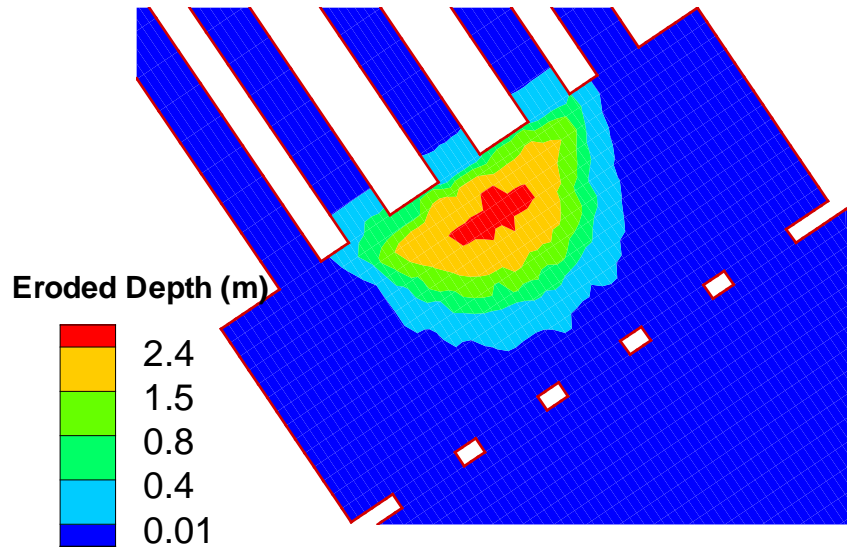
(a)   Time = 1.0 Hour (after Gate 3 release is complete)

Eroded Depth (m)

▮	2.4
▮	1.5
▮	0.8
▮	0.4
▮	0.01
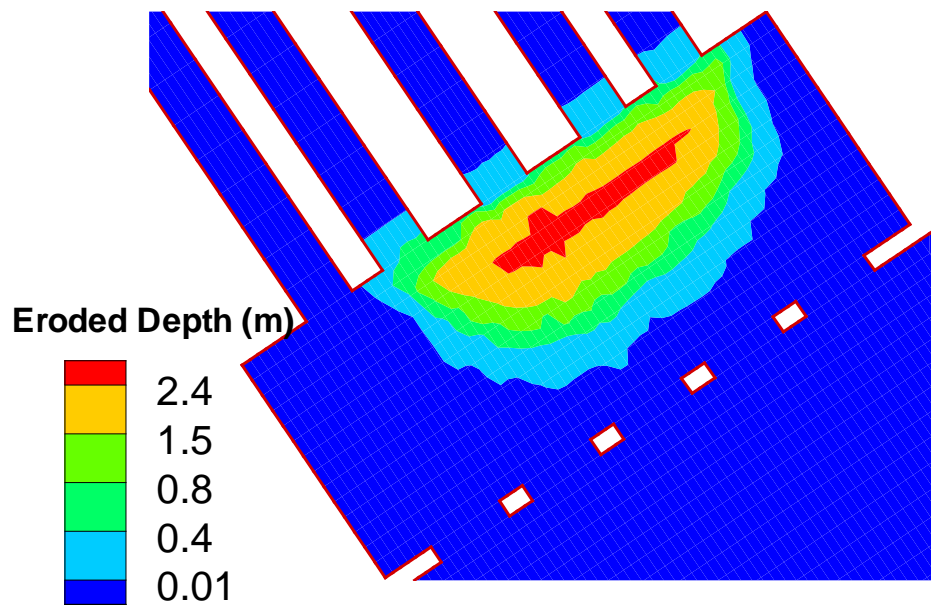
(b)   Time = 1.5 hour (after Gate 2 release is complete)

Eroded Depth (m)

■ (red)	2.4
■ (orange)	1.5
■ (green)	0.8
■ (light blue)	0.4
■ (blue)	0.01
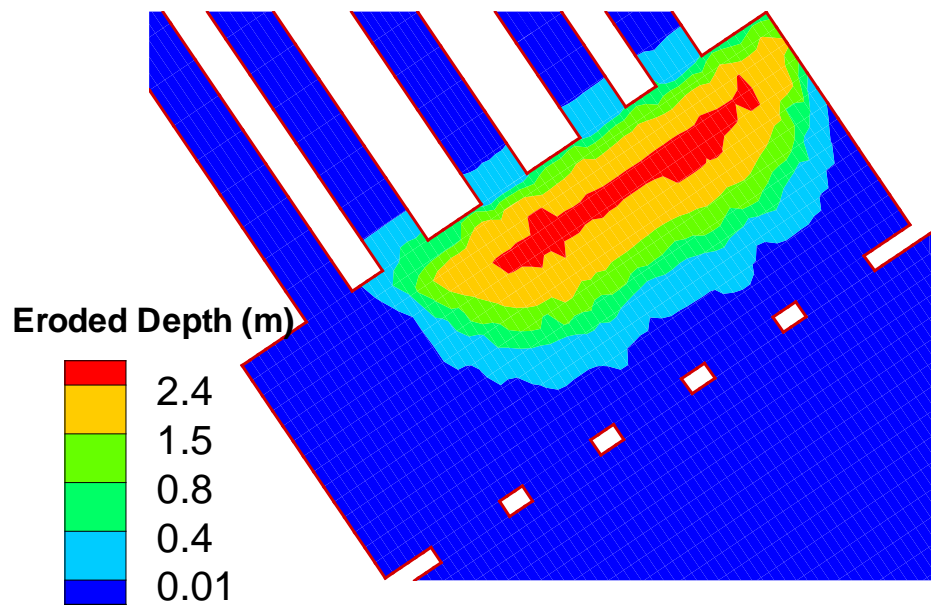
(c)   Time = 2.0 Hour (after Gate 1 release is complete)

Eroded Depth (m)

■ (red)	2.4
■ (orange)	1.5
■ (green)	0.8
■ (light blue)	0.4
■ (blue)	0.01
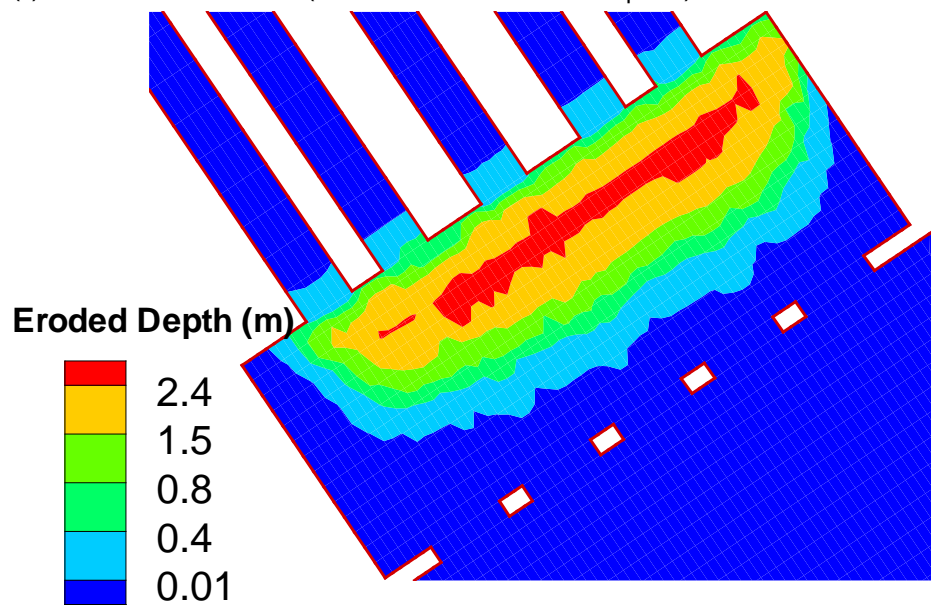
(d)   Time = 2.5 Hour (near the end of Gate 4 release)

(e)   Time = 3.5 hour (end of flushing)

Figure 23. Predicted scour zone development in time by the baseline model during the 2018 flushing (contours represent the eroded depth in meter).

4. Empirical Analysis of Pressure Flushing

To supplement the numerical model reported above and compare results against laboratory results, an empirical analysis of the expected pressure flushing cone geometry is described below.

4.1. Flow Field

The flow field upstream of an orifice in a reservoir has been studied extensively (Anayiotos et al., 1995; Shammaa et al., 2005; Bryant et al., 2008; Powell and Khan, 2014; and Vosoughi and Hajikandi, 2016). Shammaa et al. (2005) used potential flow solutions to analyze the velocity contours upstream of orifices and found that the computed decay of the velocity with distance from the orifice matched previous experimental and numerical analysis of flow fields upstream of unbounded orifices. They also found that the particular shape of the orifice is only important close to the orifice. For orifices of different geometries, they found this distance typically did not exceed 2 to 3 times of $\sqrt{A}$, where A is the area of the orifice opening. They found that maximum velocity upstream of 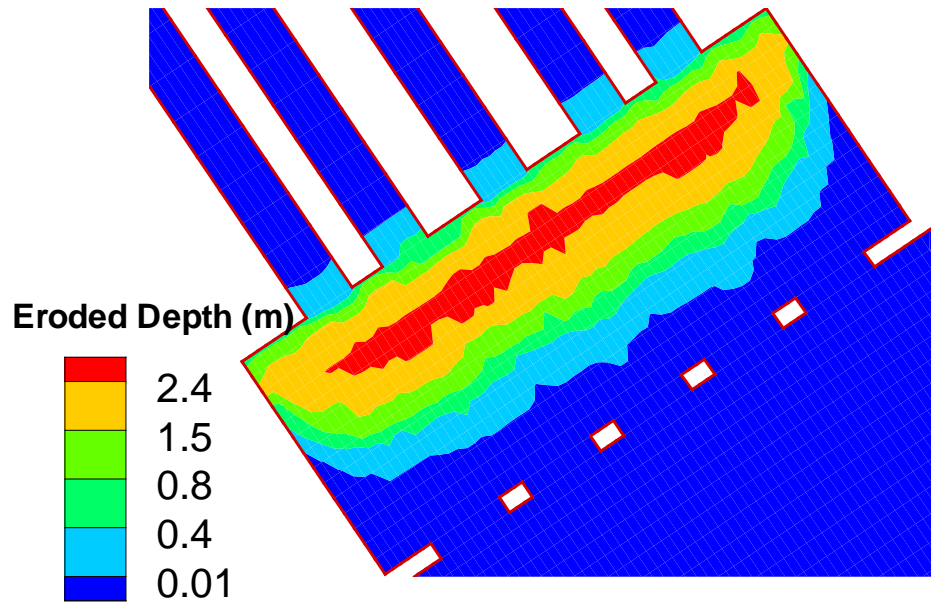an unbounded orifice where the flow depth (H) is much greater than the orifice diameter (D) ($H \gg D$) can be described by the following equation:

$$\frac{u_{max}}{U_0} = 1 - [1 + 0.25(D/x)^2]^{-0.5}$$

where:

x = distance along centerline from orifice,
D = orifice diameter, and
U_0 is the average velocity within the orifice.

This equation is only valid for $x > 0$, and the maximum velocity becomes approximately proportional to x^{-2} for x/D greater than 2. The equation also predicts that for x/D equal to 2, the maximum velocity is 3% of the average velocity at the orifice. The analysis demonstrates that velocity decreases rapidly upstream of orifices in reservoirs and therefore the effect of the orifice on erosion will be limited to a relatively small area upstream of the orifice.

Powell and Khan (2012 and 2015) studied the flow field upstream of a bounded orifice with both a fixed bed and a mobile bed. The analyzed circular orifices with the fixed bed or the initial sediment level at the elevation of the invert of the orifice. The flow field was similar to the unbounded orifice case, but the maximum velocity decreased slightly slower due to smaller area from which to draw flow into the orifice. They developed

equations of the same form as predicted from Shammaa et al. (2005), but with slight modification to coefficients:

$$\frac{u_{max}}{U_0} = 1 - [1 + a(D/x)^b]^{-c}$$

The a, b, and c values are 0.332, 1.679, and 0.515, and 0.145, 1.493, and 0.913 for the fixed bed and mobile bed cases, respectively.

4.2. Scour Analysis

An idealized conceptual figure of the scour upstream of an orifice is shown in Figure 24. The scoured area upstream of the orifice is assumed to form at a depth of D_s below the invert of the orifice. There is an approximate flat area projecting from the wall and then the scoured area is assumed to project upward at a constant angle θ.
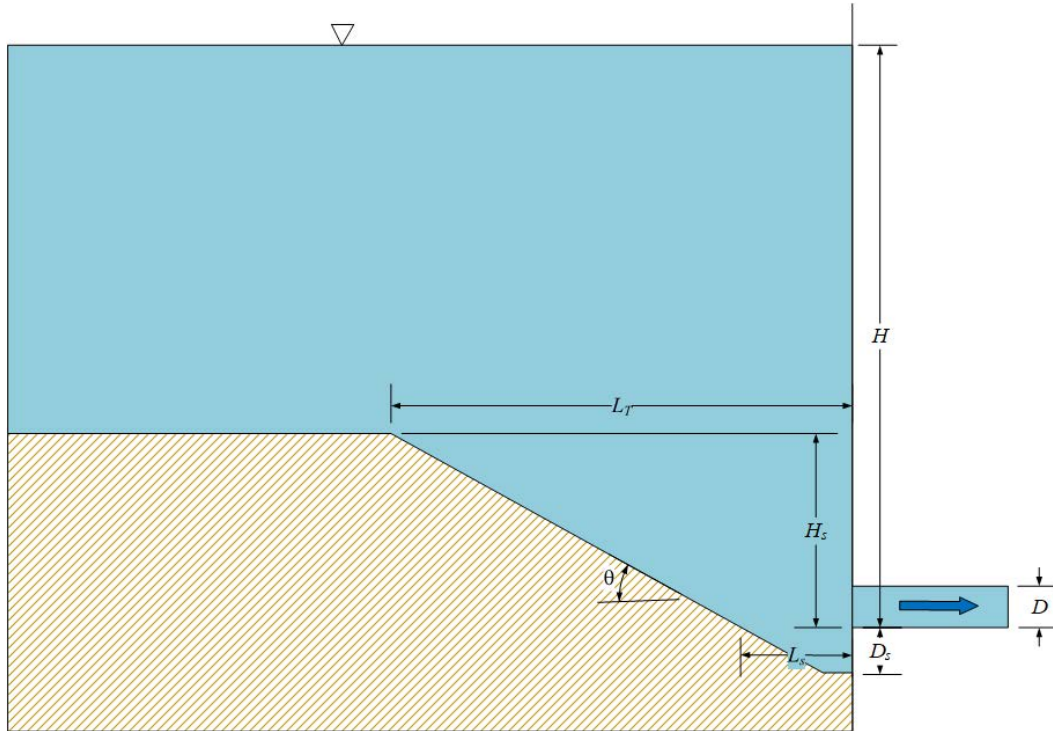

Figure 24. Idealized profile view of equilibrium scour upstream of the orifice.

Fathi-Moghadam et al. (2010) performed physical modelling of scour in non-cohesive sediment upstream of circular orifices. They found that the non-dimensional volume (V/D^3) and non-dimensional total length (L_T/D) of the equilibrium scour hole governed by the following non-dimensional equations:

44

$$\frac{V}{D^3} = 5.28 \left(\frac{U_0}{\sqrt{g(s-1)d_{50}}} \right)^{0.1} \left(\frac{H_s}{H} \right)^{0.046}$$

$$\frac{L_T}{D} = 8.19 \left(\frac{U_0}{\sqrt{g(s-1)d_{50}}} \right)^{0.1} \left(\frac{H_s}{H} \right)^{0.033}$$

Here H_s is the depth of sediment above the invert of the orifice and they did not report the depth of scour below the orifice. The first term in the equation is typically called the particle densimetric Froude Number and u is the average velocity through the orifice, s is the specific gravity and d_{50} is the median particle diameter. The experiments did not vary sediment depth (H_s) or orifice diameter (D), but had variable water depth (H),sediment diameter (d_{50}) and orifice flow velocity (u). They found that the angle of the scour cone was relative constant and was close to the angle of repose for submerged particles: θ varied between 27 to 33, 29 to 34, and 30 to 35 degrees, for the fine, medium, and coarse sand, respectively. The slope of the cone in the flow direction was only 2 to 6% larger than the slope perpendicular to the flow. Like most empirical equations, it should only be applied within the range of the experimental data upon which is was based. The value of H_s/H varied between 0.25 to 0.45, and this equation cannot be applied to estimate depth of scour when $H_s = 0$.

Kamble et al. (2017) choose to non-dimensionalize the length of scour with the water depth and developed the following equation:

$$\frac{L_T}{H} = 2.9 \left(\frac{H_s}{H} \right)^{0.51} \left(\frac{A_0}{H^2} \right)^{0.31} \left(\frac{u}{\sqrt{g(s-1)d_{50}}} \right)^{-0.44}$$

They only used one sediment size (0.25 mm) in their experiments so the dependency on the sediment size is uncertain. Because velocity is directly dependent on water depth, every non-dimensional parameter is dependent upon depth, and some hesitation is warranted in applying this equation.

Powell and Khan (2012) performed experiments in non-cohesive material with grain sizes varying between 0.29 and 0.89 mm. The orifice diameter was 15.2 cm and the head above the center of the orifice varied between 45.72 cm and 76.20 cm. The experiments were all run with $H_s = 0$. Powell and Khan (2012) performed tests and found scour hole length (L_s) varied between 1.5 D to 2.17 D, with the highest head resulting in the longer scour hole length. The depth of the scour hole varied between 0.5 D and 0.71 D, again with head resulting in the deepest scour hole. They describe the shape of the scour hole with the following non-dimensional equation:

$$\frac{d}{D_s} = \begin{cases} 1, \text{if } x/L_s < 0.15 \\ 1.2(1 - x/L_s), \text{if } 0.15 \leq x/L_s < 1 \end{cases}$$

where:

d is the local depth of scour and
x is distance from orifice.

Hajikandi et al. (2018) compared difference equilibrium scour conditions between square and circular orifices. They found very similar non-dimensional scour shapes as Powell and Khan (2012), but that the scour length was 10 to 15 percent longer for a square orifice of the small cross-sectional area as a circular orifice. Similar to Powell and Khan (2012) the length and the width of the scour hole showed weak dependency on particle size. There results also extend the results of Powell and Khan to higher values of H/D, up to a value of H/D of up to 14. The value of L_s/D varied between 1.5 to 2.8 for values of H/D from 3 to 14.

Emamgholizadeh and Fathi-Moghdam (2014) developed equations using experiment with cohesive soil and found that the densimetric Froude number was not significant compared to the bulk density of the sediment and the non-dimensional volume and total length:

$$\frac{V}{D^3} = 0.99 \left(\frac{H_s}{H}\right)^{0.59} [(1 - \eta)(s - 1)]^{-2.85}$$

$$\frac{L_T}{D} = 0.33 \left(\frac{H_s}{H}\right)^{0.4} [(1 - \eta)(s - 1)]^{-1.44}$$

where η is the sediment porosity. The side slope of the scour cones for five classes of the bulk density were measured as 55.4, 46.7, 43.2, 37.8, and 32.1 degrees with an average of 43 degrees. In their report, they noted significant discrepancy of the side slope of the scour cones with field measurements and stated that the field measurement of the Kongazhue, Bikou, Qington Gorge, Fen He, and Yan Gou Gorge reservoirs in China had measured scour cone side slopes ranging between 4 to 17° (Fang and Cao, 1996). This difference in the measured side slopes is significant and indicates that the laboratory results on scour length cannot be directly scaled to the field. It is likely that for cohesive soils the equilibrium angle of repose could be significantly different in the laboratory scale and field scale. Larger scale slumping processes could be important at the field scale than the laboratory scale.

Empirical equations will be useful in designing and evaluating expected scour in pressurized flushing scenarios. However, there are several limitations:

1. The equations may not apply outside of the range of parameters used in the development of the equation.

2. The equations do not describe all the characteristics of the scour hole.

3. The equations only apply for simple geometric conditions. Other structures added to increase scour or more complex geometries will have an unknown effect.

4. The sediment size and cohesive properties were not scaled from the field to the laboratory. Therefore, the typically non-dimensional parameters related to sediment size will be much different in the laboratory than the field.

The last point requires additional explanation. The shear strength of a soil is commonly computed as (Reclamation, 1998):

$$\tau_s = c' + (\sigma - u) \tan \phi'$$

Where:

τ_s is the shear strength of soil
c' is the effective cohesive strength
σ is the normal stress on sliding surface
u is the pore water fluid pressure
ϕ' is the internal friction angle

Assuming a uniform thickness of submerged sediment on a slope, the equation for the critical stable depth (h_c) on slope, β, is:

$$(1 - \eta)(\gamma_s - \gamma_w)h_c \tan \beta = c' + (1 - \eta)(\gamma_s - \gamma_w)h_c \tan \phi'$$

For non-cohesive soil ($c' = 0$), this equation simplifies to a simple angle of repose condition meaning that if $\beta > \phi'$, the slope is unstable and fails. The depth of sediment is not important for non-cohesive soil. For cohesive soil, it is more complicated. Typically, the sediment used in the laboratory and that is present in the field will have similar values for c' and ϕ'. Therefore, the critical depth for the same sediment slope will be similar in the laboratory as in the field. The depth of sediment in the laboratory may be below the critical depth, whereas the depth of sediment in the field is much above the critical depth. The result is that field observations of the stable slopes in the field are significantly less than in the laboratory.

A more reliable method of estimating scour hole size would be to perform two empirical analysis steps:

1. Estimate the length of the scour hole at or below the invert of the orifice (L_s) using data from Hajikandi et al. (2018) and Powell and Kahn (2012). Typical values of L_s are expected to be about 1.5 to 3 times the equivalent orifice diameter.

2. Estimate stable profile outside of scour hole using geotechnical principles. For non-cohesive soils, assume that the stable slope will be near the submerged angle of repose for that material. For cohesive soil, determine the stable profile based upon the measured effective cohesive strength and internal friction angle for that material.

The two stages of empirical analysis results from the likely scenario that there is a two-step process of evacuating sediment in front of the intake. First hydraulic forces are dominant near the intake and rather quickly remove sediment within approximately 1.5 to 3 intake diameters. Then the over-steepened area created by the sediment may fail through geotechnical processes until it reaches a stable profile.

Numerical models will be necessary to further detail and quantify the effect under a broader range of conditions than what was analyzed at the laboratory scale. For example, the change in scour patterns caused by complex geometries or operations will require numerical models. However, laboratory studies are still important to understand specific processes and verify numerical models. In general, the laboratory results likely underestimate the scour hole size because they likely underestimate the stable equilibrium slope that develops upstream of the orifice in the field.

4.3. Empirical Analysis of Cherry Creek

The above empirical method is applied to the scour cone at Cherry Creek Reservoir. The geometry of the intake has been described in the previous section and it was noted that measurements of the scour cone was only possible outside the intake tower trash racks, which is about 40 feet upstream of the orifices. The sill elevation of 4 of the 5 outlet orifices was 5504 feet, the water surface was approximately 5550 feet, and the sediment elevation far from the orifice was at approximately 5525 feet. The concrete floor of the intake tower is also at an elevation of 5504 feet and, therefore, no scour is possible below this elevation.

The 2017 measured centerline profile in the reservoir is shown in Figure 26. The measured results from 2018 are close to the 2017 survey and, therefore, the profile from 2018 is not shown. Based upon a simplified piecewise linear fit to the observed data, the length of the scoured sediment at or below the intake elevation (L_s) was limited to approximately 16 feet in front of the orifice. The length of the entire scour hole (L_T) was approximately 115 feet.

Assuming an equivalent square diameter of the Cherry Creek Outlet of 7.4 feet, the value of H/D was 6.3. The value of L_s is expected to be about 2.2 D based upon the data from Hajikandi et al. (2018) and Powell and Kahn (2012). This gives an estimated length of scour below the intake elevation, L_s, of 16 feet. Fitting a straight line to the observed stable slope of the Cherry Creek scour hole that begins at 16 feet upstream from the orifice outlet gives an approximately slope of the scour cone of 0.22, or about 12 degrees. This scour cone slope is consistent with the field measurements of Fang and Cao (1996) of field cases. The slope of the scour cone is likely approximately equal to the friction angle of the material, which is expected to be small given the high water content of the sediment (79 % water by volume). There was no measurement of the effective cohesive strength and internal friction angle for the reservoir sediment at Cherry Creek, but these measurements are highly recommended in future studies of pressure flushing.

The estimates of Emamgholizadeh and Fathi-Moghdam (2014) were the only empirical relations that apply to cohesive soil. They predict the ratio of $L_T/D = 1.3$, which assuming an equivalent circular diameter of $D = 8.3$ ft, gives $L_T = 10.8$ feet, which is less than 10% of the observed value of about 115 feet. The equations of Emamgholizadeh and Fathi-Moghdam (2014) (as well as other equations developed from laboratory data) greatly underestimate the length of the scour hole as they predict the scour hole length to be of order of the diameter of the orifice, whereas in the field, the length of the entire scour hole is over 10 times the size of the orifice. The reason for this is that there was no scaling of the geotechnical processes. The empirical equations based upon laboratory experiments do not account for the relatively shallow stable slopes of submerged, unconsolidated cohesive sediments in reservoirs.
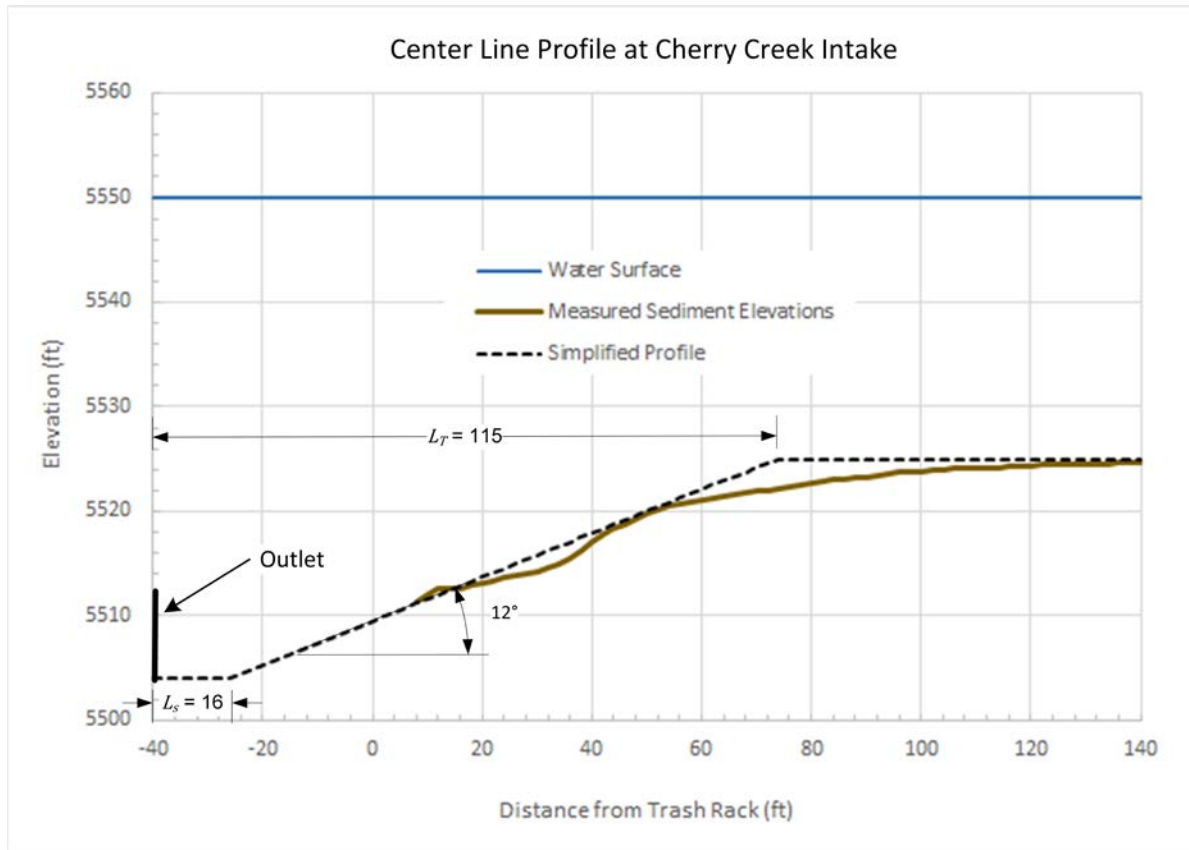
Figure 25. Measured and linear fit to the centerline sediment profile of sediment upstream of low-level outlet at Cherry Creek Reservoir. The trash rack of the intake tower is assumed to be at station 0.

5. Concluding Remarks

The numerical simulation of 2017 and 2018 pressure flushing leads to the following key findings:

- The new 3D model based on the Navier-Stokes equations and the suspended cohesive sediment transport equation is developed. The model is demonstrated to work well in simulating the pressure flushing process at the Cherry Creek Reservoir.

- The model predicted sediment release concentration is compared with the measured sediment concentration downstream in the river for both 2017 and 2018 releases. The agreement is reasonable and points to the potential of the 3D model for future pressure flushing applications.

- Pressure flushing is not an efficient large-scale sediment removal option in reservoirs. Both the 2017 (250 cfs) and 2018 (1,300 cfs) flushing operations failed to remove sediment deposits outside the intake in the reservoir. The field surveys confirmed this as the measured differences between the pre- and post-flushing bed elevations did not have detectable scours.

- Pressure flushing does produce scour cones upstream of the gates but limited to within the intake. Pressure flushing thus is effective if the objective is to clean up the sediment deposits within the intake tower and prevent clogging from occurring in front of the gates. For the actual 2017 and 2018 flushing, the numerical model predicts that the 2017 scour cones covered about 1/3rd of the intake tower horizontally while the 2018 flushing scour cones reach almost the trach rack. Geotechnical processes are likely responsible for the observed sediment slope outside the intake tower. Once the sediment from inside the intake tower is removed, some slumping of the sediment may occur and refill the area inside the intake tower. Therefore, periodic flushing should be continued to keep the gates operable and intake tower free of sediment.

The scour cone upstream of the trash rack at Cherry Creek is at an approximately equilibrium conditions, which would be expected because flushing of the gates is performed annually.

The numerical model may be used to develop an effective strategy of flushing. Based on the above results, for example, it suggests that the current 5-gate 2017 release schedule, with a maximum discharge of 250 cfs, is effective in removing the limited amount of sediments in front of the gates. If the maximum discharge would be 1,300 cfs like the 2018 release schedule, a 3-gate release, gates 3, 1 and 5, would be more efficient than the current 5-gate schedule. Other options to consider to maximum the efficiency of the flushing would be to flush every other year or to decrease the duration of the flushing. Most of the work performed by the flushing occurs immediately after the gates are opened.

This study points to future research and development direction as follows:

- A more general mesh representation of reservoirs, intakes and gates are needed in future for more general applications. The current model works with sigma mesh only.

- A more general formulation of the sediment transport is to be developed. Current implementation is limited to suspended cohesive sediment. Mixed suspended load and bedload are needed in future studies. Multi-size classes are yet to be tested and verified.

- The model is yet to be tested and validated with its ability to predict the scour cones. Physical model results would help the model validation study. Other pressure flushing field cases are to be identified in reservoirs which may have a more detailed measurement of the scour cones.

- It is recommended that future field studies at the Cherry Creek Reservoir focus on:
    (a) a detailed pre- and post-flushing sediment measurement within the intake and

    (b) sediment concentration measurement at a location closer to the release outlet. These data would help verify the 3D model more quantitatively.

- A geotechnical analysis of the stable slope of submerged cohesive sediments may need to be conducted.

6. References

Ahadpour Dodaran, A., Park, S.K., Mardashti, A., and Noshadi, M. (2012). Investigation of dimension changes in under pressure hydraulic sediment flushing cavity of storage dams under effect of localized vibrations in sediment layers. Int J Ocean Syst Eng 2(2):71–81.

Anayiotos, A.S., Perry, G.J., Myers, J.G., Green, D.W., Fan, P.O., and Nanda, N.C. (1995). A numerical and experimental investigation of the flow acceleration region proximal to an orifice. Ultrasound Med. Biol., 21(4), 501–516.

Armstrong, B. (2017). Cherry Creek Reservoir Sediment Erosion Testing Results. Technical Memorandum No. 8530-2017-22, Bureau of Reclamation, Denver, Colorado.

Basson, G. (2007). Mathematical modelling of sediment transport and deposition in reservoirs, guidelines, and case studies. ICOLD Bulletin No.140. International Commission on Large Dams, 61, avenue Kleber, 75116, Paris.

Bryant, D.B., Khan, A.A., and Nadim, N.M. (2008). Flow field upstream of an orifice. J. Hydraul. Eng., 10.1061/(ASCE)0733-9429(2008) 134:1(98), 98–104.

Cebeci, T. and Bradshaw, P. (1977). Momentum Transfer in Boundary Layers. Hemisphere, Washington DC, 319-321.

Chang, H.H., Harrison, L.L., Lee, W., and Tu, S. (1996). Numerical modeling for sediment-pass-through reservoirs. J. Hydraul. Eng., 10.1061/(ASCE)0733-9429(1996)122:7(381), 381–388.

Collins, K., Boyd, P., Shelly, J., Dombroski, D., Greimann, B. (2019). Cherry Creek Pressure Flushing Analysis. SEDHY 2019, Reno, Nevada.

Dombroski, D. (2018). Suspended Sediment Monitoring Techniques: An Investigation Coincident with the Cherry Creek Reservoir Flush. Final Report ST-2018-1893-01. Research and Development Office, Science and Technology Program, Bureau of Reclamation.

Emamgholizadeh, S. and Fathi-Moghadam, M. (2014). Pressure flushing of cohesive sediment in large dam reservoirs. J Hydrologic Engg., 19(4), 674–681. DOI: 10.1061/(ASCE)HE.1943-5584.0000859.

Emamgholizadeh, S., Bina, M., Fathi-Moghadam, M., and Ghomeyshi, M. (2006). Investigation and evaluation of the pressure flushing through storage reservoir. ARPN J Engg Appl Sci., 1(4), 7–16.

Fan J and Morris, G.L. (1992). Reservoir sedimentation. II: reservoir desiltation and long-term storage capacity. J Hydraul Eng ASCE 118(3):370–384.

Fang, H.W. and Rodi, W. (2003). Three-dimensional calculations of flow and suspended sediment transport in the neighborhood of the dam for the Three Gorges Project (TGP) reservoir in the Yangtze River. J. Hydraul. Res., 41(4), 379–394.

Fang, D. and Cao, S. (1996). An experimental study on scour funnel in front of a sediment flushing outlet of a reservoir. Proc., 6th Federal Interagency Sedimentation Conf., Las Vegas, Nevada, I-78–I-84.

Fathi-Moghadam, M., Emamgholizadeh, S., Bina, M., and Ghomeshi M. (2010). Physical modelling of pressure flushing for desilting of non-cohesive sediment, Journal of Hydraulic Research, 48:4, 509-514, DOI: 10.1080/00221686.2010.491691.

Gengsheng, W., Brethour, J., Grünzner, M., and Burnham, J. (2014). Sedimentation Scour Model, Flow Science Report 03-14 August 2014; Revised October 2014.

Hajikandi, H, Vosoughi, H, and Jamali, S (2018). Comparing the Scour Upstream of Circular and Square Orifices, International Journal of Civil Engineering (2018) 16:1145–1156, https://doi.org/10.1007/s40999-017-0269-5.

Haun, S. and Olsen, N.R.B. (2012). Three-dimensional numerical modelling of reservoir flushing in a prototype scale, International Journal of River Basin Management, 10:4, 341-349, DOI: 10.1080/15715124.2012.736388.

Huang, J. and Greimann, B.P. (2012). User's manual for SRH-1D V2.0, Sedimentation and River Hydraulics Group, Technical Service Center, Bureau of Reclamation, Denver, Colorado.

Huang, J., Greimann, B.P. and Kimbrel, S. (2019). Simulation of Sediment Flushing in Paonia Reservoir of Colorado, Journal of Hydraulic Engineering, Vol. 145, Issue 12, DOI: 10.1061/(ASCE)HY.1943-7900.0001651.

Isaac, N., Eldho, T.I., and Gupta, I.D. (2014). Numerical and physical model studies for hydraulic flushing of sediment from Chamera-II reservoir, Himachal Pradesh, India. ISH Journal of Hydraulic Engineering, 20(1), 14–23. doi:10.1080/09715010.2013.821788.

Jansson, M.B., and Erlingsson, U. (2000). Measurement and quantification of a sedimentation budget for a reservoir with regular flushing. Regul Rivers Res Manag. 16:279–306.

Kamble, S.A., Kunjeer, P.S., Sureshkumar, B., and Isaac, N. (2017). Hydraulic model studies for estimating scour cone development during pressure flushing of reservoirs, ISH Journal of Hydraulic Engineering, DOI: 10.1080/09715010.2017.1381577.

Kantoush, S.A. (2008). Experimental study on the influence of the geometry of shallow reservoirs on flow patterns and sedimentation by suspended sediments, Ph.D. thesis, École Polytechnique Fédérale de Lausanne (EPFL), Suisse.

Krone, R.B. (1962). Flumes studies of the transport of sediment in estuarial shoaling processes. Technical Report, Hydraulic Engineering Laboratory, University of California, Berkeley, California.

Lai, Y.G. (2008). SRH-2D Theory and User's Manual version 2, Technical Service Center, Bureau of Reclamation, Denver, Colorado.

Lai, Y.G. (2010). Two-Dimensional Depth-Averaged Flow Modeling with an Unstructured Hybrid Mesh. J. Hydraulic Engineering, ASCE, 136(1), 12-23.

Lai, Y.G. (2017) Development of a Three-Dimensional Hydrostatic-Assumption Model for Flow and Turbidity Current Simulation – Final Report. Sedimentation and River Hydraulics Report SRH-2018-01, Technical Service Center, U.S. Bureau of Reclamation.

Lai, Y.G., Weber, L.J., and Patel, V.C. (2003). Non-Hydrostatic Three-Dimensional Method for Hydraulic Flow Simulation - Part I: Formulation and Verification. J. Hydraulic Engineering, ASCE, vol.129(3), 196-205.

Lai, Y.G. and Bauer, T.R. (2007). Erosion analysis upstream of the San Acacia Diversion Dam on the Rio Grande River, Project Report, Technical Service Center, Bureau of Reclamation, Denver, Colorado. Lai, Y. G. and Greimann, B. P.(2010). Predicting contraction scour with a two-dimensional depth averaged model, Journal of Hydraulic Research, 48: 3, 383 — 387, DOI: 10.1080/00221686.2010.481846.

Lai, Y.G. and Greimann, B. (2012). Modeling Channel Formation on the Klamath River due to Reservoir Drawdown. 2012 United States Society of Dams Annual Meeting and Conference, New Orleans, Louisiana, April 23-27.

Launder, B.E., and Spalding, D.B. (1974). The numerical computation of turbulent flows. Comput. Methods Appl. Mech. Eng., 3, 269–289.

Liu, J., Minami, S., Otsuki, H., Liu, B., and Ashida, K. (2004). Environmental impacts of coordinated sediment flushing. J. Hydraul. Res., 42(5), 461–472.

Liu, X. (2014). New Near-Wall Treatment for Suspended Sediment Transport Simulations with High Reynolds Number Turbulence Models. J. Hydraul. Eng., 140(3), 333-339.

Madadi, M.R., Rahimpour, M., and Qaderi, K. (2017). Improving the Pressurized Flushing Efficiency in Reservoirs: an Experimental Study. Water Resour Manage, 31:4633–4647. DOI 10.1007/s11269-017-1770-y.

Malcherek, A. (2007). Sediment transport und Morphodynamik, Scriptum Institut fur Wasserwesen, Universitat Munchen, Germany.

Merkel, U.H. and Kopmann, R. (2012). "A continuous vertical grain sorting model for Telemac and Sisyphe." River Flow 2012 – Murillo (Ed.). Taylor & Francis Group, London, ISBN 978-0-415-62129-8. Pp.457-463.

Meshkati, M.E., Dehghani, A.A., Naser, G., Emamgholizadeh, S., and Mosaedi, A. (2009). Evolution of developing flushing cone during the pressurized flushing in reservoir storage. World Acad Sci Eng Technol., 58, 1107–1111.

Meshkati, M.E., Dehghani, A.A., Sumi, T., Mosaedi, A. and Meftah, M. (2012). Experimental investigation of pressure flushing technique in reservoir storages. Water and Geoscience, pp. 132–137. ISBN: 978-960-474-160-1. Reservoir sedimentation- Schleiss, eds., Taylor & Francis Group, London, ISBN 978-1-138-02675-9.

Mehta, A.J. and Partheniades, E. (1973). Depositional behavior of cohesive sediments. Technical Report No. 16. Coastal and Oceanographic Engineering Laboratory, University of Florida, Gainesville, Florida.

Morris, G.L. and Fan, J. (1997). Reservoir sedimentation handbook, McGraw-Hill, New York, New York.

Olsen, N.R.B. (2014). A three-dimensional numerical model for simulation of sediment movement in water intakes with multiblock option. Department of Hydraulic and Environmental Engineering, The Norwegian University of Science and Technology, 215 pp.

Parker, G. (2006), 1D Sediment Transport Morphodynamics with applications to Rivers and Turbidity Currents, Chapter 4, http://vtchl.uiuc.edu/people/parkerg/_private/e-bookPowerPoint/RTe-bookCh4ConservationBedSed.ppt.

Partheniades, E. (1965). Erosion and deposition of cohesive soils. Journal of the Hydraulics Devision, ASCE, Vol. 91(1), 105-139.

Powell, D. (2007). Sediment Transport Upstream of Orifices. All Dissertations. Paper 140.

Powell, D.N. and Khan, A. (2012). Scour upstream of a circular orifice under constant head. J Hydraul Res 50(1):28–34. DOI: 10.1080/00221686.2011.637821.

Powell, D.N. and Khan, A. (2015). Flow field upstream of an orifice under fixed bed and equilibrium scour conditions. J Hydraul Eng. 141(2): 04014076. DOI:10.1061/(ASCE)HY.1943-7900.0000960 04014076.

Reclamation (1998). Earth Manual Part 1, Third Edition, Earth Sciences and Research Laboratory Geotechnical Research, Technical Service Center, Bureau of Reclamation. Denver, Colorado.

Reza Madadi, M., Rahimpour, M. and Qaderi, K. (2016). Sediment flushing upstream of large orifices: An experimental study, Flow Measurement and Instrumentation 52 (2016) 180–189, http://dx.doi.org/10.1016/j.flowmeasinst.2016.10.007.

Shammaa, Y., Zhu, D.Z., and Rajaratnam, N. (2005). Flow upstream of orifices and sluice gates. J. Hydraul. Eng., 10.1061/(ASCE)0733-9429 (2005)131:2(127), 127–133.

Shen H.W. (1999). Flushing sediment through reservoirs. Journal of Hydraulic Research, 37 (6), 743-757.

Stumpp, S. (2001). Investigations on Modeling of Large River-Bed Roughness, M.S. Thesis, University of Stuttgart and IIHR.

Talebbeydokhti, N. and Naghshineh, A. (2004). Flushing sediment through reservoirs. Iran J Sci Technol, Trans B, 28(B1):119–136.

van Rijn, L.C. (1984). Sediment transport, Part III: Bed forms and alluvial roughness. J. Hydr. Engrg., 110(12), 1733–1754.

van Rijn, L. C. (1993). Principles of sediment transport in rivers, estuaries, and coastal seas, Aqua Publications, Amsterdam, The Netherlands.

Vosoughi, H., Hajikandi. H. (2016). Experimental Investigation of Scour Upstream of a Square Orifice under Constant Head. Journal of Civil and Environmental Engineering, Volume 46, Issue 2, Summer 2016.

White, W. R. (2001). Evacuation of sediments from reservoirs. ThomasTelford Publishing, London. http://dx.doi.org/10.1680/eosfr.29538.

Wu, W., Rodi, W., and Wenka, T. (2000). 3D Numerical Modeling of Flow and Sediment Transport Open Channels. J. Hydraul. Eng., 126(1), 4-15.

Xue, W., Huai, W., Li, Z. et al. (2013). Numerical simulation of scouring funnel in front of bottom orifice. J Hydrodyn 25, 471–480. https://doi.org/10.1016/S1001-6058(11)60386-8.

Zyserman, J. and Fredsøe, J. (1994). Data Analysis of Bed Concentration of Suspended Sediment. Journal of Hydraulic Engineering, 120(9), 1021–1042.